Title: The collision of two genomes threatens global food security

Authors: Henry L. North *[1,2], Gabriela Montejo-Kovacevich *[1,3,4], Douglas Amado *[1,5], Ian A. Warren [1], Marek Kucka [6,7], Abby Williams [1,8], Yingguang Frank Chan [6,7], Tom Walsh [9], Alberto Soares Corrêa [1,5], Celso Omoto [5], Chris D. Jiggins ‡[1]

* These authors contributed equally to this work

‡ Materials and correspondence: cj107@cam.ac.uk

Affiliations:

1 Department of Zoology, University of Cambridge, Downing Street, Cambridge CB2 3EJ, UK

2 Girton College, University of Cambridge, Huntingdon Road, Cambridge CB3 0JG UK

3 Evolutionary Biology Centre, Department of Ecology and Genetics, Science for Life Laboratory, Uppsala University, Uppsala, Sweden

4 King's College, University of Cambridge, King's Parade, Cambridge, CB2 1ST UK

5 Department of Entomology and Acarology, Escola Superior de Agricultura Luiz de Queiroz, Universidade de São Paulo, Av Padua Dias 11, 13418-900 Piracicaba, SP, Brazil

6 Friedrich Miescher Laboratory of the Max Planck Society, 72076 Tübingen, Germany

7 Groningen Institute for Evolutionary Life Sciences (GELIFES), University of Groningen 9747AG Groningen, The Netherlands

8 Present Address: Department of Biology, University of Oxford, South Parks Road, Oxford OX1 3EL

9 CSIRO Environment, Black Mountain Innovation Precinct, Clunies Ross St., Acton, 2601, ACT, Australia.

Summary paragraph

Human activity alters selection pressures and redistributes biodiversity, creating opportunities for hybridization when different species come into secondary contact. It is now well-established that ancient hybridization plays an important role in adaptive radiation [1], but its role in recent anthropogenic adaptation remains unclear. We investigated this in a study of hybridizing native and invasive *Helicoverpa* moths in Brazil, which are among the most economically damaging crop pests globally. Native *H. zea* has recently evolved Bt resistance and is better adapted to maize as a host plant, while invasive *H. armigera* is resistant to pyrethroid pesticides and is better adapted to soybean. Using a decade-long time series of 975 genomes from both species, we demonstrate rapid, bidirectional adaptive introgression of structural variants that cause resistance to two distinct pesticides. In one direction, a pyrethroid resistance gene from *H. armigera* (*CYP337B3*) is now almost fixed in native *H. zea*. In the other direction, ~30% of recently-sampled invasive *H. armigera* carry a *H. zea*-derived trypsin repeat cluster. Using controlled crosses, we show that this trypsin repeat cluster confers resistance to Bt (Cry1Ac) soy in the *H. armigera* genomic background. Thus, hybridization has combined *H. armigera* adaptation to soy with H. zea Cry1Ac resistance to facilitate exploitation of Brazilian Bt soy monoculture — a vast anthropogenic habitat exceeding the area of Germany. Our results show that the combinatorial mechanisms that produce biodiversity can also drive rapid anthropogenic adaptation on ecological timescales, with consequences for global food security.

Main text

Introduction

Human activity imposes natural selection at unprecedented scales through changes in land use, climate, and chemical exposure. At the same time, humans are redistributing biodiversity across the globe, resulting in the introduction of non-native species to novel ecological conditions. As a consequence, biological invasion events — where ecological opportunists establish and spread in new environments — are occurring at an accelerating rate [2]. As species' distributions shift, once-isolated lineages can come into secondary contact and may hybridize. This confluence of strong natural selection and admixture can create conditions for evolutionary rescue, with far-reaching implications from conservation to food security [3,4].

It is now well-established that introgression between previously isolated lineages can produce novel hybrid trait combinations that drive adaptive diversification over thousands or millions of years [1]. Central to this 'combinatorial mechanism' is the amalgamation of modular genetic architectures into new configurations that facilitate the occupation of new niche space. Since admixture introduces adaptive variants at high frequency, which have already been optimised by selection in parental linages, adaptation can proceed rapidly. For example, hybridization brought together two wing colour developmental switches selected in independent *Heliconius* butterfly linages, resulting in a novel recombinant phenotype underlying adaptation and reproductive isolation [5]. Similarly, novel traits required for ecological divergence in *Helianthus* sunflowers resulted from a combination of alleles that arose in distinct ancestral

lineages [6]. A handful of studies have shown that anthropogenic activity can lead to unidirectional adaptive introgression [7–10]. Given the role of combinatorial evolution in ancient adaptive diversification, this begs the question: could similar mechanisms drive adaptation at even shorter timescales relevant to anthropogenic change? Cases of secondary contact between native and invasive species are particularly tractable systems in which to investigate this question.

Secondary contact between previously isolated noctuid moth species of the genus *Helicoverpa* present a remarkable natural experiment in rapid adaptation. In 2013 *Helicoverpa armigera* was detected as an invasive species in Brazil, where it encountered its sister species, *H. zea*. While *H. armigera* has a broad distribution spanning most of the eastern hemisphere, *H. zea* — which diverged in allopatry 1.5-2MYA — is native to the Americas [11]. The two species are among the world's most destructive agricultural pests, and the establishment of *H. armigera* in South America resulted in annual economic damage of around $US 10^7 [12]. Highly polyphagous larvae feed on the reproductive structures of major crops including soy, maize, and cotton [13]. The species' broad-scale pesticide resistance, short generation times (up to 11/yr), high fecundity (>1,000 eggs/female), and long-distance dispersal (up to 40 km/night) enable explosive population growth [14–17]. Despite being difficult to distinguish morphologically, the two species are separated by strong prezygotic behavioural and mechanical barriers, which makes them difficult to cross in captivity [18]. It was therefore a surprise when genomic data revealed occasional interspecific hybridization in Brazil [19,20]. This resulted in adaptive introgression of the *de novo* chimeric pyrethroid pesticide resistance gene *CYP337B3* from invasive *H. armigera* to native *H. zea* populations in

96 Brazil and subsequently North America [21,22]. Previous work hinted at a single bout of
97 locus-specific introgression [21]. However, the two species display complementary
98 ecological adaptations, leading to speculation that further introgression could drive
99 ongoing adaptation to control measures [20,23].
100
101 Invasive *H. armigera* primarily affects soybean and cotton — the former being the most
102 abundant crop in Brazil, comprising 47.3×10^6 hectares in the 2024-25 crop season, an
103 area exceeding the total size of Germany [24,25]. However, following its outbreak in 2013,
104 *H. armigera* damage to cotton and soy has been effectively suppressed through the
105 widespread use of soy crops genetically modified to express *Bacillus thuringiensis* (Bt)
106 toxins such as Cry1Ac [26,27]. In contrast, native *H. zea* cannot complete its lifecycle on
107 soy; it primarily affects the second most-abundant Brazilian crop — maize — and is
108 tolerant to Cry toxins, which have been expressed in North American maize and cotton
109 since the late 1990s [28]. The coexistence of these species raises the question of whether
110 hybridization could combine the Bt tolerance of native *H. zea* with the soy adaptation of
111 invasive *H. armigera* to facilitate adaptation to Bt soybean monoculture in Brazil.
112
113 Here, we study the recent adaptive consequences of hybridization using a decade-long
114 whole-genome time series of 975 field-collected moths from across Brazil, combined
115 with the genomes of a further 149 individual offspring from a cross between Bt-resistant
116 and susceptible *H. armigera*. This unique dataset captures the complete time course of
117 the invasion and its aftermath. We reveal ongoing hybridisation and bidirectional gene
118 flow, identify a trypsin gene cluster introgressed from *H. zea* into *H. armigera*, and show
119 experimentally that it confers resistance to Cry1Ac-expressing soy in the *H. armigera*

genomic background. These architectures are produced by the sorting of alleles at major-effect loci independently optimised by anthropogenic selection in native and invasive pests. These results provide a rare insight into rapid adaptation over ecological timescales through selection on novel genomic architectures for pesticide resistance.

Results

Outcome of secondary contact

We first sought to characterise the outcome of secondary contact between these species over time by quantifying individual-level ancestry across the full set of Brazilian *Helicoverpa* samples (*n*=975, Extended Data Table 1). There are various possible outcomes to hybridization. At one extreme, the two species could collapse into a single hybrid swarm, predicting a pattern of increased intermediate-ancestry individuals over time. At the other extreme, reinforcing selection would predict declining intermediate-ancestry individuals and declining ancestry heterozygosity over time. To distinguish between these patterns, we used non-admixed samples of both species to assign ancestry (Fig. 1A)

Most Brazilian samples clustered with reference *H. armigera* and *H. zea* samples in principal component space, with a minority of intermediate individuals (Fig. 1B). Ancestry proportions estimated using diagnostic loci (Fig. 1C) and genotype likelihoods (Fig. 1D, Extended Data Fig 1) confirm that most samples primarily carry ancestry from one species or the other. Early-generation hybrids were rare. Nevertheless, the vast majority of samples were advanced-generation back-crosses carrying a small proportion of ancestry from the alternative species. Patterns of ancestry across space

143 and time indicate an established mosaic hybrid zone throughout Brazil (Extended Data
144 Figs. 2A,B) consistent with previous reports [29]. The dominant ancestry of samples was
145 predicted by the crop on which they were sampled: *H. armigera* on soy and cotton, and
146 *H. zea* on maize (Extended Data Fig. 3). Proportionally more early-generation hybrids
147 (those with <95% ancestry of either species) were found where the two species
148 overlapped spatially and temporarily (Extended Data Fig. 2C).
149
150 The frequency of advanced-generation back-crosses in early samples, combined with
151 the lack of spatial or temporal change in ancestry, confirms that *H. armigera* had
152 established in South America well before its official discovery [30]. Although the ancestry
153 average heterozygosity decreased over time, early-generation hybrids were still found in
154 recent years, indicating rare but ongoing hybridization (Fig. 1D, Extended Data Fig. S4).
155 In summary, the data show stable coexistence of the two species, but with extensive
156 interspecific gene flow: most individuals carry a small proportion of alleles from the
157 alternate species. We next sought to identify those introgressed alleles.
158

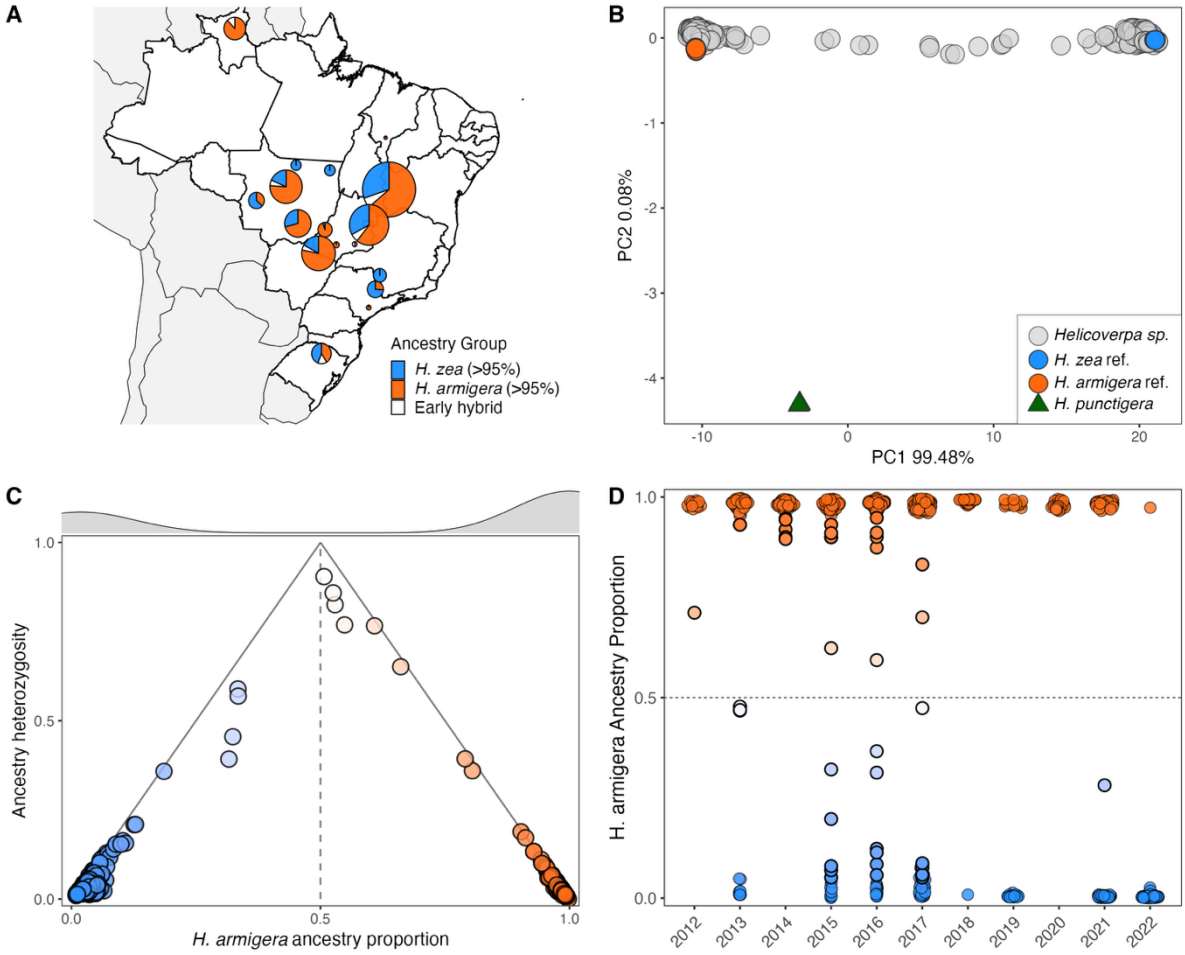

Figure 1) (A) Sample sites of individual genomes across all years (*N*=975). Circle size corresponds to per-site sample size, colour corresponds to ancestry group. **(B)** Principal components analysis (PCA) of reference non-admixed samples and Brazilian samples. **(C)** Ancestry proportion and heterozygosity of Brazilian samples in Call Set 2. **(D)** *H. armigera* ancestry proportion of Brazilian samples in the genotype likelihood dataset for each year.

Genome-wide patterns of introgression

To identify loci with disproportionate representation of the alternate species' ancestry, we assigned individuals to species using an ancestry proportion threshold of 0.5 (Fig. 1C) and measured excess allele sharing with reference non-admixed heterospecific samples using the statistic f_d. We used two test topologies, which allowed us to

172 distinguish between introgression from South American *H. armigera* to South American
173 *H. zea* and introgression in the opposite direction (see Methods). Readers familiar with
174 earlier *Helicoverpa* reference assemblies should note that the assembly used here,
175 generated by Jin *et al*. [15], numbers chromosomal scaffolds by size (see Extended Data
176 for synteny comparisons showing the corresponding chromosomes). Aggregating
177 samples across the time-series, the genome-wide average signature of introgression
178 was similar for both directions (Extended Data Fig. 5), but the chromosomal distribution
179 of the introgression signal differed significantly between the two species (Extended
180 Data Figs. 6,7). Local reductions in F_{ST} and d_{XY} in a sympatric comparison of the two
181 species (in Brazil), relative to the allopatric comparison (non-admixed native-range
182 populations), confirm introgression in Brazil (Extended Data Figs. 8, 9). From invasive *H.*
183 *armigera* to native *H. zea*, the introgression signal is concentrated at the *CYP337B3*
184 locus on chromosome 5, confirming previous results (Extended Data Fig. 6). Nucleotide
185 diversity decreased over time in both donor and recipient species around *CYP337B3*,
186 clearly demonstrating adaptive introgression (Extended Data Fig. 10). By contrast,
187 introgression in the other direction is distributed across most chromosomes, with
188 notable 'plateau' patterns consistent with locally reduced recombination on
189 chromosomes 21, 24, and 26 (Extended Data Fig. 7). Although synteny between the two
190 species is high, comparisons within and between both species confirm the
191 introgression of inversion polymorphisms on these chromosomes (Extended Data Figs.
192 11, 12, 13, 14, 15, 16). A subset of samples sequenced using haplotagging confirm the
193 presence of these inversions, and reveal other structural variants (SVs) that were not
194 introgressed (Extended Data Fig. 17). Intriguingly the haploblock introgressed from *H.*
195 *zea* represents the ancestral orientation in all cases (Extended Data Fig. 18). PCA-based

196 inversion genotyping showed that all *H. armigera* individuals carrying the *H. zea*
197 inversion allele were heterozygous (Extended Data Figs. 19, 20), suggesting a lack of
198 strong selection. To narrow down potential instances of adaptive introgression, we next
199 identified introgression signals that increased consistently over time.
200

201 ***Temporal patterns of introgression***

202 We divided samples into three timepoints comprising approximately equal individual
203 sample sizes (Extended Data Fig. 21). For each we calculated f_d as above, as well as the
204 positive change in the introgression signal over the two intervals: $\left(f_{d_{t3}} - f_{d_{t2}}\right) +$
205 $\left(f_{d_{t2}} - f_{d_{t1}}\right)$. As expected, gene flow from *H. armigera* to *H. zea* increased over time at
206 loci surrounding *CYP337B3* on chromosome 5 (Fig. 2A, Extended Data Figs. 22, 23, 24).
207 At this locus, *H. armigera* ancestry increased rapidly among *H. zea* over the first time
208 interval, reaching near-fixation in recently collected samples. On the remainder of
209 chromosome 5, *H. armigera* ancestry declined over time in *H. zea* (Extended Data Fig.
210 24). This result is consistent with decoupling of *CYP337B3* from linked *H. armigera*
211 alleles over successive generations, declining in frequency either through drift or
212 selection against interspecific incompatibilities. This phenomenon is predicted in
213 theory and can be inferred retrospectively, but is rarely observable directly.
214

215 From native *H. zea* to invasive *H. armigera*, there was no detectable change in the
216 frequency of *H. zea* inversion haploblocks on chromosomes 21, 24, and 26, suggesting
217 that these structural variants are not under directional selection (Extended Data Fig.
218 25). Instead, introgression primarily increased over time in a narrow region of
219 chromosome 12 in samples collected after 2018 (Fig. 2B, Extended Data Figs. 26, 27,

28). A cluster of tandem repeat trypsin genes (digestive proteases) mapped to the chromosome 12 locus showing the greatest increase in introgression from *H. zea* to *H. armigera* across the whole genome (Extended Data Fig. 27). In North American *H. zea*, this cluster has previously identified and associated with field-evolved resistance to the *Bt* toxin Cry1Ac [28,31]. More generally, trypsins have been repeatedly implicated in Bt resistance in lepidopterans [32–34]. We confirmed the presence of this introgressed structural variant by using a subset of linked-read haplotagged samples collected early in the time series: *H. zea* samples show a pattern of tag-sharing diagnostic of tandem duplication at the trypsin locus, while *H. armigera* samples did not (Fig. 2C). Although recently-collected *H. armigera* samples were not haplotagged, the introgressed repeat cluster could be inferred through changes in local depth of coverage over the time course (Fig. 2D). At the *Trypsin* locus, normalised depth of coverage in *H. zea* was elevated and constant between 2012 and 2022, but increased over time in *H. armigera* coincident with increased use of Bt soy in Brazil (Fig. 2D). Notably, 4 of 8 Brazilian *H. zea* samples collected in 2005 displayed the diagnostic peak in read depth, indicating polymorphism prior to the deployment of Bt in Brazil. Together these results point to selection for a structural variant conferring Bt resistance in Brazilian *H. zea* between 2005 and 2012, followed by recent introgression into *H. armigera*. We next aimed to test the hypothesis that this introgressed structural variant confers a novel resistance phenotype in Brazilian *H. armigera* exposed to Bt soy.

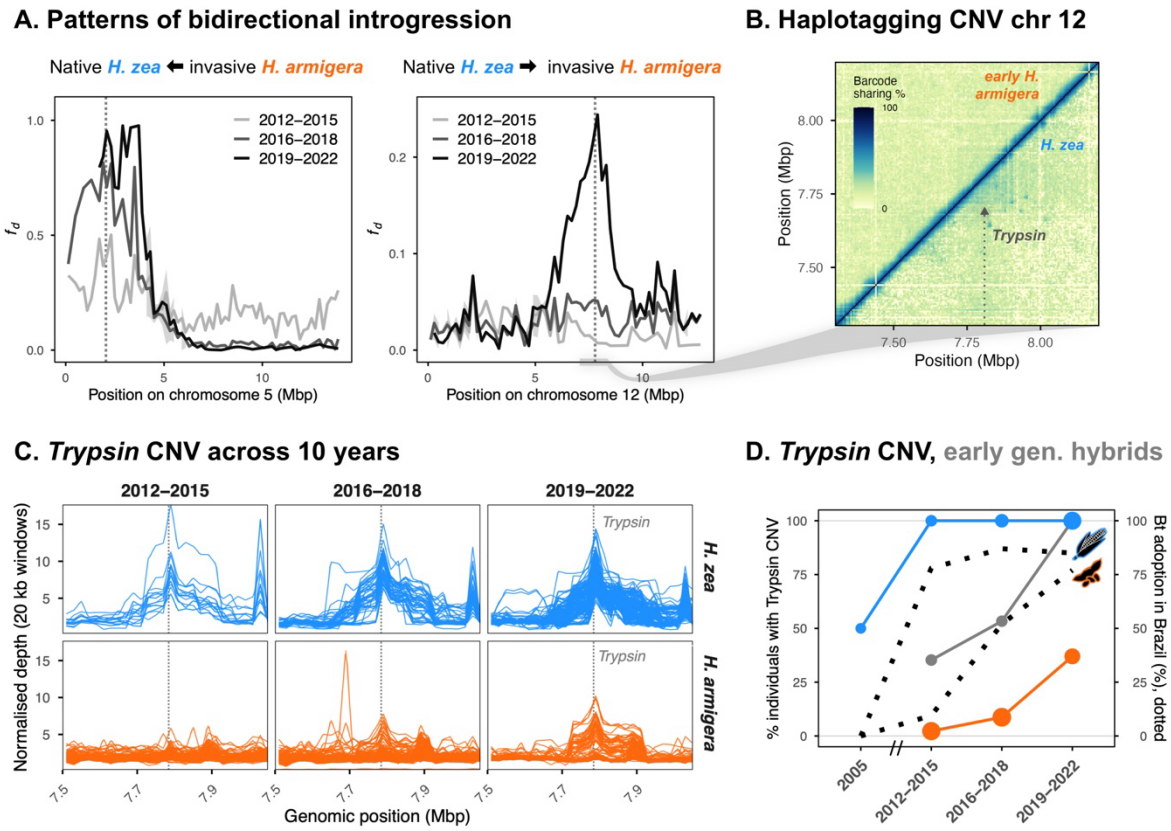

Figure 2. (A) Left panel: f_d using the topology (((ZEA, ZEA_BRAZIL), ARM)), PUN), indicative of introgression from *H. armigera* to *H. zea*, shown for chromosome 5 for individuals split into three temporal sets. Right panel: f_d using the topology (((ARM, ARM_BRAZIL), ZEA)), PUN), indicative of introgression from *H. zea* to *H. armigera*, shown for chromosome 12 for individuals split into three temporal sets. **(B)** Haplotag barcode sharing in *H. zea* samples collected early in the time-series (bottom right corner) and *H. armigera* collected early in the time-series (top left corner). A triangular shape consistent with a tandem duplication is evident at the introgressed trypsin locus in *H. zea* samples. **(C)** Normalised depth of coverage on chromosome 12 for *H. zea* samples (top panel) and *H. armigera* samples (bottom panel), where each individual is one line. Increases in relative depth of coverage in *H. armigera* appear over time, consistent with introgression. **(D)** Detection of the repeat cluster using depth of coverage. Circle size indicates individual sample size for *H. armigera* (orange), early-generation hybrids (grey) and *H. zea* (blue). Dashed lines: Bt adoption in Brazil; percentage of total Brazilian soy area with Bt, as reported by de Freitas Bueno *et al.* [35] and percentage of Brazilian maize area with Bt, as reported by Schuster *et al.* [36].

261 **A *H. zea* trypsin repeat cluster confers *Bt* resistance in wild *H.***

262 ***armigera***

263 To identify the loci underlying Bt resistance in Brazilian *H. armigera*, we collected wild
264 individuals in 2018 and artificially selected those that survived on leaf discs of Bt
265 soybean expressing Cry1Ac (see Methods). Tolerant and susceptible lines were crossed
266 to produce an F2 population segregating for Cry1Ac resistance (Fig. 3A, 3B). Using
267 whole-genome resequencing data for data for 149 F_2 individuals plus their parents and
268 grandparents, we confirmed that all samples were *H. armigera* (minimum *H.* armigera
269 ancestry proportion = 0.966, mean = 0.975; Extended Data Fig. 29) and carried out
270 quantitative trait locus (QTL) mapping for Cry1Ac resistance (Extended Data Fig. 30,
271 Extended Data Table 2). This revealed two major effect loci on chromosomes 12 and 5,
272 which showed no evidence of epistatic interactions (Fig. 3D, Extended Data Figs. 31, 32,
273 Extended Data Tables 2, 3, 4, 5).

274

275 We next quantified introgression signals as above for the *H. armigera* QTL samples.
276 Remarkably, both major-effect loci showed a localised enrichment of *H. zea* ancestry
277 among individuals that survived Cry1Ac treatment (Fig. 3C, Extended Data Fig. 33). This
278 confirms predictions that locally adapted *H. zea* variants would enhance *H. armigera*
279 fitness in Brazil [20,23]. However, only one of the two QTL showed evidence of introgression
280 in field-collected samples. At the chromosome 5 QTL (LOD= 6.48, p=3.29×10^{-7}) there
281 were no obvious signs of interspecific introgression in wild-caught *H. armigera*
282 (Extended Data Fig. 33) despite its additive effect on Cry1Ac resistance. In contrast,
283 confidence intervals for the chromosome 12 QTL (LOD= 8.80, p=1.57×10^{-9}) overlapped
284 with the *Trypsin* repeat cluster (Fig. 3C), which we identified as the locus with the

strongest increase in introgression through time in the wild (Fig. 2A). *Trypsin* CNV presence/absence genotyping based on depth of coverage at this locus showed that individuals with the CNV were significantly more likely to be Bt-resistant (Fig. 3D). In wild *H. armigera*, this same locus showed extreme genetic differentiation over time relative to the genome-wide average (Fig. 3E, Extended Data Fig. 10). Therefore, laboratory selection for Cry1Ac resistance in Brazilian *H. armigera* had the effect of enriching for existing introgressed *H. zea* structural variant alleles, thereby replicating the adaptive introgression observed in wild populations. Interestingly, this QTL showed signs of underdominance in the presence of Bt, where fitness is lowest in heterozygotes (Extended Data Fig. 32). Despite this apparent barrier to introgression at low frequencies, the introgressed trypsin allele frequency in *H. armigera* closely tracks the rollout of Bt soy in Brazil [35] (Fig. 3D). Although the CNV was fixed in *H. zea* collected from 2012 onwards, samples from 2005 were polymorphic. This suggest that *H. zea* evolved resistance relatively recently, likely through gene flow from North American *H. zea* populations exposed to Cry-expressing maize and cotton since the late 1990s, followed by adoption in Brazilian maize since 2007 (Fig. 3D).

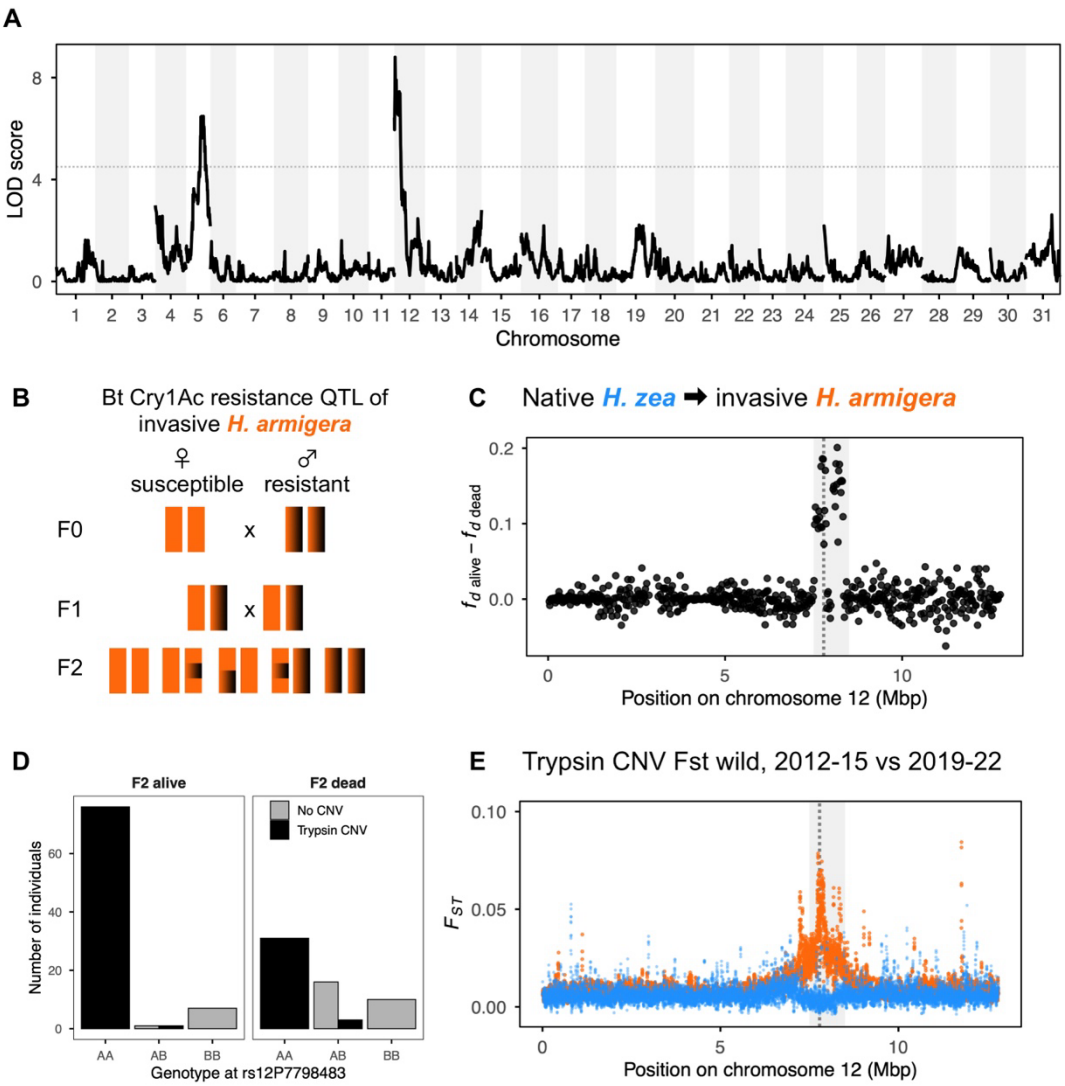

Figure 3: (A) Logarithm of odds (LOD) score for quantitative trait locus (QTL) mapping of Cry1Ac resistance in Brazilian *H. armigera*. Two major effect loci are identified on chromosomes 12 and 5 **(B)**. Intercross design for the linkage mapping experiment presented in 3A. **(C)** Difference in the signal of *H. zea* allele sharing between alive and dead individuals. In both cases f_d was calculated using the topology (((ARM, QTL_SAMPLE), ZEA)), PUN). Dashed line indicates the trypsin locus, with grey shaded regions indicating the QTL confidence intervals. *H. armigera* samples that survived when exposed to Cry1Ac carried an excess of *H. zea* alleles on a haplotype directly overlapping with the QTL confidence interval. **(D)** Count of individuals in the intercross that survived or died when exposed to Cry1Ac, split by genotype and detection of the trypsin CNV based on excess normalised depth of coverage. The A allele, associated with survival in homozygotes, corresponds to the trypsin CNV. **(E)** Genetic differentiation (F_{ST} calculated using genotype likelihoods) on chromosome 12 between samples collected early and late in the time-series. *H. armigera* is shown in orange; *H. zea* is shown in blue. *H. armigera* samples show excess differentiation at the trypsin locus (dashed line; QTL confidence intervals shaded in grey), consistent with introgression over time. *H. zea* shows reduced differentiation at this locus compared to the rest of the chromosome, consistent with a selective sweep.

Discussion

Together these findings indicate persistent but permeable species boundaries upon secondary contact between native and invasive agricultural pests, resulting in bidirectional adaptive introgression of structural variants conferring resistance. In addition to adaptive introgression of *CYP337B3* from invasive *H. armigera* to native *H. zea*, more recent adaptive introgression in the other direction has introduced Bt (Cry1Ac) resistance alleles to ~30% of the invasive *H. armigera* population. Thus, hybridization has generated a novel combination of traits — soy host plant adaptation in *H. armigera* and Bt resistance selected in *H. zea* — which together enable colonisation of an expansive anthropogenic habitat: Brazilian Bt soybean monoculture.

Just as ancient hybridization can combine old adaptive variants to facilitate adaptive diversification over thousands of years, these results demonstrate how contemporary hybridization can assemble independently selected alleles into a single admixed genome, resulting in adaptation over ecological timescales. Notably, the recombined adaptive variants do not need to be 'ancient': the trypsin allele underlying Cry1Ac resistance was polymorphic in Brazilian *H. zea* as recently as 2005, and has only recently been selected — likely through exposure to Cry-expressing maize and cotton in North America [28]. Thus, anthropogenic change not only drives rapid adaptation through selection on standing variation, but can also promote hybridization, which can further accelerate adaptation. Consequently, in this system, resistance to control measures has evolved in two major agricultural pests through bidirectional adaptive introgression over the course of less than a decade.

346 The practical outcome of hybridization between *H. armigera* and *H. zea* is the 'worst of
347 both worlds': two distinct agricultural pests are now resistant to control measures, and
348 show greater adaptive potential. In the case of *H. zea*, the pyrethroid resistance gene
349 *CYP337B3* had reached near-fixation in the most recently collected samples. This large
350 pyrethroid-resistant Brazilian source population of *H. zea* is a biosecurity threat to the
351 two largest maize producing agro-economies: the United States, where the spread *H.*
352 *armigera*-derived *CYP337B3* in *H. zea* is already causing an increase in pyrethroid
353 control failures [37], and China, where *H. zea* is non-native. In the case of *H. armigera*,
354 approximately 30% of samples collected between 2019 and 2022 carried Cry1Ac
355 resistance alleles. An additional *H. zea*-derived Cry1Ac resistance QTL on chromosome
356 5 was present in wild-caught *H. armigera*, and is expected to spread in the population
357 given its additive phenotypic effect. These results provide an early warning of Cry1Ac-
358 resistant *H. armigera* in Brazil. More broadly, Brazilian *H. armigera* pose an increasingly
359 imminent biosecurity threat to the U.S., where the species has not yet spread. Transport
360 of Brazilian *H. armigera* back into its native range is also a biosecurity concern. For
361 example, Australian *H. armigera* populations harbour monogenic resistance mutations
362 for the Bt toxin Vip3Aa [38]. This raises the possibility of recombinant trans-Pacific *H.*
363 *armigera* genotypes conferring resistance to multiple Bt toxins, potentially threatening
364 'pyramiding' strategy of multi-toxin Bt crop use.
365
366 Overall, a combination of serial-sampled genomic data and linkage mapping has
367 revealed a combinatorial mechanism driving rapid adaptation. The outcome of
368 interspecific hybridization can range from rapid adaptation to demographic collapse,
369 ultimately depending on the genetic architecture and ecological contingency of hybrid

fitness [39]. In systems such as this, admixture has enabled the sharing of adaptive variation between distinct and competing species. For pests and pathogens, such rapid evolutionary rescue presents a challenge to food security and multidrug resistance. For some threatened taxa, the same process could facilitate persistence. Recognising hybridization as a driver for adaptation on anthropogenic timescales will be essential for understanding evolutionary responses to global change.

Main text References

1. Marques, D. A., Meier, J. I. & Seehausen, O. A Combinatorial View on Speciation and Adaptive Radiation. Trends Ecol. Evol. 34, 531–544 (2019).
2. Seebens, H., Meyerson, L. A. & Rahlao, S. J. Trends and status of alien and invasive alien species. in Thematic Assessment Report on Invasive Alien Species and their Control of the Intergovernmental Science-Policy Platform on Biodiversity and Ecosystem Services (eds. Roy, H. E., Pauchard, A., Stoett, P. & Tanara, R. T.) (IPBES secretariat, Bonn, Germany, 2023).
3. Kreiner, J. M. The genetic architecture and spatiotemporal dynamics of adaptation across human-modified landscapes. New Phytologist https://doi.org/10.1111/NPH.70520 (2025) doi:10.1111/NPH.70520.
4. Jørgensen, P. S. et al. Antibiotic and pesticide susceptibility and the Anthropocene operating space. Nat. Sustain. 1, 632–641 (2018).
5. Wallbank, R. W. R. et al. Evolutionary Novelty in a Butterfly Wing Pattern through Enhancer Shuffling. PLoS Biol. 14, e1002353 (2016).
6. Rieseberg, L. H. et al. Major Ecological Transitions in Wild Sunflowers Facilitated by Hybridization. Science (1979). 301, 1211–1216 (2003).
7. Oziolor, E. M. et al. Adaptive introgression enables evolutionary rescue from extreme environmental pollution. Science (1979). 364, 455–457 (2019).
8. Song, Y. et al. Adaptive Introgression of Anticoagulant Rodent Poison Resistance by Hybridization between Old World Mice. Current Biology 21, 1296–1301 (2011).
9. Leroy, T. et al. Adaptive introgression as a driver of local adaptation to climate in European white oaks. New Phytologist 226, 1171–1182 (2020).
10. Kreiner, J. M. et al. Rapid weed adaptation and range expansion in response to agriculture over the past two centuries. Science (1979). 378, 1079–1085 (2022).
11. Behere, G. T. et al. Mitochondrial DNA analysis of field populations of Helicoverpa armigera (Lepidoptera: Noctuidae) and of its relationship to H. zea. BMC Evol. Biol. 7, 1–10 (2007).
12. Bueno, A. de F. & Sosa-Gómez, D. R. The Old World Bollworm in the Neotropical Region: The Experience of Brazilian Growers with Helicoverpa Armigera. Outlooks on Pest Management 25, 261–264 (2014).

13. Cunningham, J. P. & Zalucki, M. P. Understanding Heliothine (Lepidoptera: Heliothinae) Pests: What is a Host Plant? J. Econ. Entomol. 107, 881–896 (2014).
14. Fitt, G. P. The Ecology of Heliothis Species in Relation to Agroecosystems. Annu. Rev. Entomol. 34, 17–53 (1989).
15. Jin, M. et al. Adaptive evolution to the natural and anthropogenic environment in a global invasive crop pest, the cotton bollworm. The Innovation 4, 100454 (2023).
16. Jones, C. M. et al. Genomewide transcriptional signatures of migratory flight activity in a globally invasive insect pest. Mol. Ecol. 24, 4901–4911 (2015).
17. Jones, C. M., Parry, H., Tay, W. T., Reynolds, D. R. & Chapman, J. W. Movement Ecology of Pest Helicoverpa: Implications for Ongoing Spread. https://doi.org/10.1146/annurev-ento-011118 (2018) doi:10.1146/annurev-ento-011118.
18. Hardwick, D. The corn earworm complex. Memoirs of the Entomological Society of Canada 97, 5–247 (1965).
19. Anderson, C. J., Tay, W. T., McGaughran, A., Gordon, K. & Walsh, T. K. Population structure and gene flow in the global pest, Helicoverpa armigera. Mol. Ecol. 25, 5296–5311 (2016).
20. Anderson, C. J. et al. Hybridization and gene flow in the mega-pest lineage of moth, Helicoverpa. Proceedings of the National Academy of Sciences 201718831 (2018).
21. Valencia-Montoya, W. A. et al. Adaptive Introgression across Semipermeable Species Boundaries between Local Helicoverpa zea and Invasive Helicoverpa armigera Moths. Mol. Biol. Evol. 37, 2568–2583 (2020).
22. North, H. L. et al. Rapid Adaptation and Interspecific Introgression in the North American Crop Pest Helicoverpa zea. Mol. Biol. Evol. 41, (2024).
23. Mallet, J. Invasive insect hybridizes with local pests. Proc. Natl. Acad. Sci. U. S. A. 115, 4819–4821 (2018).
24. Ministério do Desenvolvimento Agrário e Agricultura Familiar. Informações Agropecuárias: Soja. (2025).
25. Toloi, M. N. V., Bonilla, S. H., Toloi, R. C., Silva, H. R. O. & Nääs, I. de A. Development Indicators and Soybean Production in Brazil. Agriculture 2021, Vol. 11, Page 1164 11, 1164 (2021).
26. Dourado, P. M. et al. High Susceptibility to Cry1Ac and Low Resistance Allele Frequency Reduce the Risk of Resistance of Helicoverpa armigera to Bt Soybean in Brazil. PLoS One 11, e0161388 (2016).
27. Horikoshi, R. J. et al. Large-scale assessment of lepidopteran soybean pests and efficacy of Cry1Ac soybean in Brazil. Scientific Reports 2021 11:1 11, 15956- (2021).
28. Taylor, K. L., Quackenbush, J., Lamberty, C., Hamby, K. A. & Fritz, M. L. Polygenic response to selection by transgenic Bt-expressing crops in wild Helicoverpa zea and characterization of a major effect locus. BMC Genomics 2024 25:1 25, 1247- (2024).
29. Cordeiro, E. M. G. et al. Hybridization and introgression between Helicoverpa armigera and H. zea: An adaptational bridge. BMC Evol. Biol. 20, 1–12 (2020).
30. Sosa-Gómez, D. R. et al. Timeline and geographical distribution of Helicoverpa armigera (Hübner) (Lepidoptera, Noctuidae: Heliothinae) in Brazil. Sociedade

Brasileira De Entomologia https://www.biodiversitylibrary.org/part/171801 (2016).

31. Legan, A. W. et al. Mismatch between lab-generated and field-evolved resistance to transgenic Bt crops in Helicoverpa zea. Proc. Natl. Acad. Sci. U. S. A. 121, e2416091121 (2024).

32. Li, H. et al. Characterization of cDNAs encoding three trypsin-like proteinases and mRNA quantitative analysis in Bt-resistant and -susceptible strains of Ostrinia nubilalis. Insect Biochem. Mol. Biol. 35, 847–860 (2005).

33. Liu, C. et al. Cis-mediated down-regulation of a trypsin gene associated with Bt resistance in cotton bollworm. Scientific Reports 2014 4:1 4, 1–6 (2014).

34. Oppert, B., Kramer, K. J., Beeman, R. W., Johnson, D. & McGaughey, W. H. Proteinase-mediated insect resistance to Bacillus thuringiensis toxins. Journal of Biological Chemistry 272, 23473–23476 (1997).

35. Bueno, A. de F. et al. Over 10 Years of Bt Soybean in Brazil: Lessons, Benefits, and Challenges for Its Use in Integrated Pest Management (IPM). Neotrop. Entomol. 54, (2025).

36. Schuster, I., Rodrigues, R. A. D. O. & Linares, E. Genetically modified corn in Brazil: historical, results and perspectives. International Journal of Maize & Sorghum 21, (2022).

37. Nufer, M. I. et al. Anatomy of a pest control failure: introgression of cytochrome P450 337B3 alleles from invasive old-world bollworm into native corn earworm (Lepidoptera: Noctuidae). Journal of Insect Science 24, 94 (2024).

38. Bachler, A. et al. Disruption of HaVipR1 confers Vip3Aa resistance in the moth crop pest Helicoverpa armigera. PLoS Biol. 23, e3003165 (2025).

39. Schneemann, H. Fitness Landscapes, Genetic Interactions, and the Fitness of Hybrids. (University of Cambridge, Cambridge, 2023).

489 # Methods

490 ## Sample collection, DNA extraction, library preparation, and

491 ## sequencing

492 For samples in 'batch 1', *Helicoverpa* adults were collected throughout Brazil as part of
493 routine monitoring. For all other sample batches, *Helicoverpa* larvae were collected
494 from agricultural regions across Brazil and sent to the Arthropod Resistance Laboratory
495 at the Luiz de Queiroz College of Agriculture, University of São Paulo, as part of routine
496 monitoring of susceptibility to chemical insecticides and Bt proteins during the 2012–
497 2022 crop seasons (Fig. 1A, Extended Data Table 1; SISBIO numbers: 65052, 75582 and
498 61824; SisGen numbers: A792B04 and R1EA05A; TTM/ATM number: 1014273). For each
499 field-collected sample, we performed both molecular identification to distinguish *H.*
500 *armigera* from the native *H. zea*, following the PCR–RFLP protocol described by Behere
501 *et al.* [1]. Field-collected larvae were reared for at least one generation under controlled
502 laboratory conditions (25 ± 1°C, 70 ± 10% RH, and a 14h photophase). Between three
503 and seven days after adult emergence, individuals from each population in each season
504 were individually placed in 1.5mL Eppendorf tubes containing 98% ethanol and stored
505 at –20 °C.

506

507 Genomic DNA was extracted from 2mm wide segments of the thorax using Kučka and
508 Chan's high molecular weight magnetic bead DNA extraction protocol [2] . DNA
509 concentration was quantified using a Qubit™ fluorometer (Invitrogen, USA), and low-
510 concentration samples were re-extracted or excluded. For a subset of samples, DNA
511 was extracted either from the thorax or leg using the CTAB extraction protocol and

512 resuspended in 50 µl of Milli-Q water [3]. For this subset, DNA quality control was initially
513 assessed by visual inspection on a 0.8% (w/v) agarose gel, followed by
514 spectrophotometric and fluorometric analyses, and each sample was evaluated using a
515 NanoDrop spectrophotometer to detect potential contaminants and an agarose gel to
516 assess DNA integrity, and subsequently quantified using a Qubit fluorometer.
517
518 For all samples, sequencing libraries were prepared via a tagmentation based approach
519 using a homemade tn5 transposase as per Picelli *et al.* [4]. Prior to pooling, DNA
520 concentration and insert size were assessed using a Qubit™ fluorometer and
521 TapeStation (Agilent Technologies) respectively. Equal amounts of each library were
522 pooled together, and then sequenced (150bp paired-end) using an Illumina NovaSeq
523 6000 (Novogene UK).
524
525

526 **Haplotagging Library Construction and Sequencing**

527 Haplotagging libraries were prepared following the protocol of Meier *et al.* [5]. In total, we
528 analysed 93 individuals: 63 *H. armigera*, 16 *H. zea*, and 14 putative hybrids collected in
529 Brazil between 2012–2018. Genomic DNA was extracted from thorax tissue and
530 normalised to 0.15 ng μl^{-1} in 10 mM Tris (pH 8). Libraries were constructed in 96-well
531 plates. Each sample received 1.2 µl of haplotagging beads (~0.9 million beads carrying
532 one of 885K barcodes), 30 µl WASH buffer (20 mM Tris pH 8, 50 mM NaCl, 0.1 % Triton-
533 X100), 10 µl of 5× tagmentation buffer (50 mM TAPS pH 8.5, 25 mM $MgCl_2$, 50 % DMF),
534 and 25 µl of 0.6 % SDS to strip Tn5 after tagmentation.

535 For amplification, one-tenth of the bead–DNA complexes from each of the 96 samples
536 was pooled within eight-tube strips, and subsequently collapsed into four final pools.
537 After placing the bead pools on a magnetic rack, residual buffer was removed and
538 replaced with 20 µl of 1× Lambda Exonuclease buffer supplemented with 10 U
539 exonuclease I and 5 U Lambda exonuclease (NEB). Beads were incubated at 37 °C for
540 30 min, washed twice with 150 µl WASH buffer, and resuspended for PCR. Libraries
541 were amplified using Q5 High-Fidelity DNA polymerase (NEB) in four 25 µl reactions per
542 pool, using 10 µM TruSeq-F (AATGATACGGCGACCACCGAGATCTACAC) and TruSeq-R
543 primers (CAAGCAGAAGACGGCATACGAGAT). Cycling conditions were: 72 °C for 10
544 min; 98 °C for 30 s; followed by 10 cycles of 98 °C for 15 s, 65 °C for 30 s, and 72 °C for
545 60 s. PCR products were pooled, size-selected using AMPure XP beads, quantified by
546 Qubit, and normalised to 2.5 nM using 10 mM Tris (pH 8.0, 0.1 mM EDTA).

547 Pooled libraries were sequenced on an Illumina HiSeq 3000, using a 150 + 13 + 12 + 150
548 (R1 + i7 + i5 + R2) configuration. This design produces 13-bp i7 and 12-bp i5 index reads
549 corresponding to haplotag plate and well barcodes.

550 Bioinformatics

551 **Read mapping**

552 The mapping and variant-calling pipeline was executed using Snakemake [6]. We mapped
553 reads to the highest-quality available *H. armigera* reference assembly, generated from a
554 sample collected in north-western China [7]. After trimming fastq files using Fastp v0.23 [8],
555 and bwa mem v0.7.12 [9] was used to map reads. SAMtools v1.10 [10] was used to sort and
556 index the resulting bam files. Duplicates were marked and removed using Picard's
557 MarkDuplicates v2.9.2 [11].

558

559 **Sequencing Depth Profiling and Sexing**

560 To characterise genome-wide and chromosome-specific sequencing depth per
561 individual, we used mosdepth v0.3.3 and d4tools v0.3.4 to compute and summarise
562 base-level coverage from mapped reads. All analyses were conducted on BAM files
563 previously aligned to the reference genome. Depth was computed per base using
564 mosdepth with the following parameters: --mapq 20 to restrict to confidently mapped
565 reads, --d4 to output in compressed D4 format, and --fast-mode to skip insertions and
566 deletions. Each sample was processed in parallel using 4 threads. To obtain per-
567 chromosome depth summaries, we ran d4tools stat with the -s median and -s mean
568 options on the .d4 files. This produced one summary file per sample containing median
569 and mean depth values per chromosome. These values were used in downstream
570 analyses to infer sex chromosome copy number, normalise depth across the genome,
571 and examine population-level variation in coverage patterns.

572 **Haplotagging Read Processing, Mapping and SV detection**

573 Raw BCLs were converted to FASTQ using bcl2fastq v2.20 with: --use-bases-mask
574 Y150,I13,I12,Y150 --minimum-trimmed-read-length 1 --mask-short-adapter-reads 1 --
575 create-fastq-for-index-reads (Illumina). Haplotag barcodes consist of four 6-bp
576 sequences embedded in the FASTQ read name. Barcode strings were assigned to the
577 BX tag following Meier *et al.* [5], allowing one mismatch when an unambiguous closest
578 match existed. Adapter trimming and quality filtering (if required) were conducted prior
579 to alignment. Reads were mapped to the H. armigera reference genome (GenBank:
580 GCA_030705265.1) using BWA-MEM2, retaining barcode information using the –C flag.

581 Alignments were coordinate-sorted with samtools, and PCR duplicates were marked
582 with Picard MarkDuplicates using: READ_ONE_BARCODE_TAG=BX
583 CREATE_INDEX=true. This preserves molecule-level identity during duplicate marking.
584 All resulting BAMs were inspected to confirm correct propagation of BX:Z: tags and
585 uniform coverage across windows. These processed, barcode-aware BAM files were
586 used for downstream analyses.

587 We identified candidate structural variants (SVs) using Wrath v2024.03, a tool designed
588 to detect large-scale SVs from linked-read sequencing data by quantifying barcode
589 sharing between genomic windows [12]. Analyses were performed separately for each
590 chromosome using the BAM files with barcodes encoded in the BX tag. To run Wrath,
591 we provided a list of BAM files per group, the chromosome of interest and a fixed
592 window size of 10 kb. Wrath calculates the Jaccard index of shared barcodes between
593 each pair of non-overlapping windows, producing a barcode-sharing matrix for each
594 chromosome.

595 **Variant calling for call sets 1 and 2**

596 In addition to genotype-liklihood-based methods, some analyses made use of variant
597 calls. Variants were called using GATK HaplotypeCaller v4.3 [13]. To improve genotyping
598 calling performance, and to enable comparison with reference populations, a diverse
599 array of publicly available *Helicoevrpa* sp. was used, in addition to samples from
600 closely related species. Before filtering, a total of 1366 individuals were included for
601 genotyping. These included 1017 newly sequenced Brazilian *Helicoverpa* samples; 124
602 native-range *H. armigera* reported by Jin *et al.* [7], of which 20 were used as reference non-
603 admixed *H. armigera*; a further 31 *Helicoverpa* samples reported by Anderson *et al.* [14]

604 including 7 *H. punctigera* individuals as an outgroup; 13 *H. zea* sampled in 2002
605 reported by Taylor *et al.* [15] for use as reference non-admixed samples; 4 *H. zea* samples
606 collected in the US in 2019 by North *et al.* [16]; 62 *Helicoverpa* samples collected in North
607 America by North *et al.* (2026); 112 Brazilian *Helicoverpa* samples collected by Valencia
608 Montoya *et al.* [17] and Anderson *et al.* [14]; and three additional outgroups: *Chloridea*
609 *subflexa* and *C. virescens* generated by Guo *et al.* [18] and *H. assulta* generated by Xu *et al.*
610 [19].
611
612 Some newly sequenced samples previously sequenced by Valencia Montoya *et al.* [17] or
613 Anderson *et al.* [14]. Of these duplicates, we retained whichever had the highest depth.
614 After removing such duplicates, we retained a total of included 1128 Brazilian
615 *Helicoverpa* samples, including those used for linkage mapping.
616
617 GATK CombineVCFs was used to merge GVCF files across individuals and
618 GenotypeGVCFs was used to call genotypes jointly across samples. In order for
619 genotyping to be computationally feasible, each of the 31 chromosomes were divided
620 into 20 equally sized intervals. Genotyping was carried out in parallel per-interval before
621 concatenating intervals into a single VCF file.
622 Two filtering approaches were used to generate call set 1 and call set 2, respectively.
623
624 **Filtering: call set 1**
625 Call set 1 was used to quantify introgression, and was applied to Brazilian *Helicoverpa*
626 samples, and reference non-admixed groups (see Quantifying Introgression, below).
627 First, bcftools v1.19 was used to retain only biallelilc SNPs from Brazilian *Helicoverpa*

samples with an autosomal mean depth of coverage of at least 5X, as calculated using vcftools v 0.1.17. Reference non-admixed samples were also required to meet this criteria, with the exception of 5 *H. punctigera* samples (M0236, M0239, M0244. M0245, and M0263) which fell marginally below an average of 5X. From here, all samples GATK VariantFiltration and SelectVariants (v4.2.5.0) were used to flag and exclude variants according to the following conditions: SOR > 3.0, FS > 60.0, MQRankSum < -20.0, MQRankSum > 20.0, ReadPosRankSum < -10.0, ReadPosRankSum > 10.0. Invariant sites were then excluded. Next, vcftools v 0.1.17 was used to apply the following conditions: --max-missing 0.75 --minQ 20 --min-meanDP 5 --minDP 5. Next, individual-level genotype-level filters were applied using a custom python script (filter1.py), which retained genotypes with a depth in the range between $\frac{1}{5}x$ and $5x$ where x is the mean autosomal depth of coverage for that individual calculated using vcftools, and otherwise set genotype calls to missing data ('./.'). Finally, after the introduction of missing data through the genotype-level filter, vcftools --max-missing 0.75 was re-applied. This resulted in a VCF file of 628 individuals containing 25,319,153 sites across all chromosomes.

Filtering: call set 2

Call set 2 consisted of more individuals and a less-stringent filter with respect to the proportion of missing data and the per-individual mean depth of coverage. Call set 2 was only used for individual-level summary statistics (see Ancestry Proportion and Ancestry Heterozygosity, below). Filter 2 was only to autosomal loci for Brazilian *Helicoverpa* samples and reference non-admixed samples with a depth of at least 0.5X using mosdepth (see above). First, GATK VariantFiltration and SelectVariants was used

652 to apply the following conditions: SOR > 3.0, FS > 60, MQRankSum < -20.0,
653 MQRankSum > 20.0, ReadPosRankSum < -10.0, ReadPosRankSum > 10.0. Next,
654 vcftools was used to apply the following filters: -max-missing 0.5 --minQ 20 --min-
655 meanDP 5 --minDP 5. Next, individual-level genotype filters were applied using a
656 custom python script (filter2_4_v2.py) using the same logic as that used for filter 1:
657 retaining genotypes with a depth in the range between $\frac{1}{5}x$ and $5x$ where x is the mean
658 autosomal depth of coverage for that individual. Finally, vcftools --max-missing 0.5 was
659 re-applied. This resulted in a VCF file of 1,014 individuals comprising 31,013,075
660 polymorphic autosomal loci.

661 **Ancestry proportion ancestry heterozygosity using call set 2**

662 The ancestry proportion (AP, equivalent to the hybrid index) and ancestry heterozygosity
663 (AH, equivalent to the interclass heterozygosity) were calculated using sites that were
664 fixed differences when comparing reference non-admixed *H. armigera* and reference
665 non-admixed *H. zea* by applying scripts adapted from Liu *et al.* [20] to call set 2.
666 Specifically, the AP is the per-sample proportion of alleles derived from *H. armigera*,
667 while the AH is the proportion of genotypes that are heterozygous. AH is therefore
668 equivalent to Fitzpatrick's interclass heterozygosity H_I and Turelli and Orr's p_H, while the
669 AP is directly comparable to the hybrid index calculated in genomic or geographic cline
670 analyses [21,22]. The AP correlated strongly with the ANGSD ancestry proportion (Extended
671 Data Fig. 1).

672

673 **Quantifying introgression using call set 1**

674 Given the availability of samples collected in locations and times when admixture had
675 never been reported (native-range *H. armigera* collected in North-Western China and *H.*

676 *zea* collected in North America in 2002, and *H. punctigera*), the following 'backbone'
677 phylogeny could be used: (ARM, ZEA), PUN. Using the ANGSD *H. armigera* ancestry
678 proportion to assign Brazilian *Helicoverpa* samples to *H. armigera* (>0.5) or *H. zea*
679 (<0.5), introgression could therefore be measured in both directions. We reasoned that
680 gene flow from invasive *H. armigera* to native Brazilian *H. zea* would result in an excess
681 of ABBA patterns relative to BABA in the following topology: (((ZEA, ZEA_BRAZIL), ARM)),
682 PUN). In the reverse direction, gene flow from native *H. zea* to invasive Brazilian *H.*
683 *armigera* would result in an excess of ABBA patterns relative to BABA in the following
684 topology: (((ARM, ARM_BRAZIL), ZEA)), PUN). Using this framework, the summary
685 statistic f_d [23] were calculated in 200kbp windows with at least 500 informative sites, and
686 20kbp windows with at least 200 usable sites. This was done for both test topologies
687 using Python scripts described in Martin *et al.* [23]. For window-based analyses, outlier
688 regions were defined as the upper 5th and 1st percentile of the f_d distribution.
689
690 Samples were divided into three timepoints comprising approximately equal individual
691 sample sizes (Extended Data Fig. 21). For each, the positive change in the introgression
692 signal over the two intervals was calculated as $\left(f_{d_{t3}} - f_{d_{t2}}\right) + \left(f_{d_{t2}} - f_{d_{t1}}\right)$.
693
694 Additionally, F_{ST} and d_{XY} were calculated for the same window sizes using the same
695 informative site threshold for two comparisons: an allopatric comparison (reference
696 non-admixed *H. armigera* and *H. zea*) and a sympatric comparison (Brazilian *H.*
697 *armigera* and *H. zea*). This was used to confirm the expectation that regions
698 introgressed in sympatry should show high f_d values and reduced F_{ST} and d_{XY} in
699 sympatry relative to allopatry.

700

701 **Mapping and genotyping inversion polymorphisms using call set 1**

702 DGENIES, which implements Minimap2, was used to generate genome-wide dot plot
703 synteny maps and MAF alignment files [24,25]. Only query and reference alignments of at
704 least 200kbp, and assembly scaffolds of at least 1Mbp, were retained. Synteny plots
705 (Extended Data Figs. 11, 12, 13, 14, 15, 16) were generating using R scripts described by
706 Kim *et al.* [26]. This was applied to intra- and inter-specific comparisons between *H.*
707 *armigera* and *H. zea* reference assemblies [7,27–30].

708

709 To assign inversion genotypes, PCA was calculated with PLINK using only loci within the
710 inversion regions of interest, as defined by the breakpoints mapped with Minimapper2.
711 Clusters were assigned to genotypes manually according to expected genotypic states
712 under the model proposed in Extended Data Fig. 18.

713

714 **Population Structure Inference from Genotype Likelihoods**

715 Population structure was inferred using genotype likelihoods computed in ANGSD
716 v0.935, followed by principal component analysis and admixture estimation using
717 PCAngsd v1.10. BAM files were grouped by population subset and filtered to retain sites
718 where ≥80% of individuals were genotyped. Genotype likelihoods were computed using
719 the GATK model (-GL 2) with base and mapping quality filters (-minQ 20, -minMapQ 30),
720 and with major alleles and allele frequencies estimated internally (-doMajorMinor 1, -
721 doMaf 1). Depth filters were scaled by the number of individuals: a minimum of 2×N and
722 a maximum of 5×mean depth×N. Genotype likelihoods were output in Beagle format (-
723 doGlf 2) and analysed with PCAngsd using the following non-default parameters:

number of ancestral populations fixed at K=2, shrinkage of the covariance matrix enabled, and no LD pruning. PCAngsd was run with --admix, --beagle, and inferred admixture proportions and principal components directly from the genotype likelihoods.

Admixture proportions using genotype likelihoods

Population structure and ancestry proportions were inferred using PCAngsd v1.10, which estimates covariance matrices and admixture components directly from genotype likelihoods. Genotype likelihoods were computed in ANGSD using the filtering scheme described above, but without downsampling sites; instead, we retained all genomic positions that passed quality filters and for which ≥75% of individuals in the population had at least one informative read (ANGSD option -minInd, set to 0.75 × *N*). This approach preserves the full genomic signal while excluding sparse or poorly covered sites that could bias covariance estimation. For each population, genotype likelihoods were exported in Beagle format after applying minimum allele frequency (-minMaf 0.05), site-quality, and depth filters, as well as a population-specific maximum-depth threshold to avoid inflated likelihoods from read pile-ups. Concatenated per-chromosome likelihood files were used as input to PCAngsd, which jointly estimates the covariance matrix under a probabilistic framework and computes individual ancestry coefficients without the need for called genotypes. The resulting admixture coefficients were taken from the *.admix* output and used as continuous ancestry estimates for all downstream analyses, including Fst contrasts and temporal structuring.

Detection of hybridisation hotspots across space and time

To test whether hybrids overlap in space and time with regions where both species (*H. armigera* and *H. zea*) were sampled at a given timepoint, we clustered individuals by geographic proximity within each year. Specifically, we applied hierarchical clustering using average linkage on geographic coordinates (latitude and longitude), grouping individuals sampled within the same year into spatial clusters with a maximum pairwise distance of 100 km (using the Haversine distance). This approach accounted for the high dispersal ability of Helicoverpa moths while ensuring sufficient sample sizes within clusters. For each year-specific cluster, we recorded the number of individuals assigned to each of three ancestry categories: H. armigera (>95% inferred ancestry), H. zea (<5%), and early-generation hybrids (intermediate ancestry). A cluster was classified as an area of species overlap if it contained at least three individuals of each parental species (H. armigera and H. zea). We then quantified the number of clusters with and without overlap, and with and without hybrids, and visualised their distributions as a stacked barplot. To test whether overlap between the parental species was associated with the presence of hybrids, we performed a Chi-squared test of independence with Yates' continuity correction.

Genetic Differentiation Analyses using genotype likelihoods

Genetic differentiation between population pairs was estimated using the site allele frequency (SAF)–based FST framework implemented in ANGSD v0.935 and realSFS. Individuals were grouped into predefined groups by time ranges (12-15, 16-18, 19-22) and species' ancestries (considered one of the two study species in their ancestry proportion was >95%). Genotype likelihoods were computed using the SAMtools model (-gl 1) with filters for read and mapping quality (-minQ 20, -minMapQ 30), and base

alignment quality recalculation enabled (-baq 2). Sites were further filtered to remove low-quality reads (-remove_bads 1) and counts were generated using -doCounts 1. SAFs were estimated per population using -dosaf 1, with ancestral and reference sequences both specified (-anc, -ref). To avoid bias from over-represented sites, a maximum depth threshold scaled by population size and average depth was applied (-setMaxDepth), calculated as 5×mean depth×N. A joint two-dimensional site frequency spectrum (2D-SFS) was estimated between population pairs using realSFS, based on their .saf.idx likelihood files. This 2D-SFS was then used to compute FST indices with realSFS fst index, and genome-wide sliding window FST values were calculated with realSFS fst stats2 using a window size of 5 kb and step size of 1 kb for plotting.

Nucleotide Diversity and Neutrality Statistics using genotype likelihoods

Nucleotide diversity (θ statistics) was estimated for each predefined population using the ANGSD–realSFS workflow. For each population, genotype likelihoods were recalculated as described above and per-population site allele frequency (SAF) likelihoods were generated using -dosaf 1, with the reference genome also specified as the ancestral state. To avoid inflation of diversity estimates due to read pile-ups, a population-specific maximum depth threshold was applied using -setMaxDepth, calculated as 5 × mean depth × number of individuals in the population. For each chromosome (1–31), an unfolded per-chromosome site frequency spectrum (SFS) was first inferred with *realSFS*, restricted to the corresponding genomic interval. This SFS was then used to convert SAF likelihoods into θ-estimators with *realSFS saf2theta*, generating per-site estimates of pairwise nucleotide and Tajima's *D* among others. Genome-wide summary statistics for each chromosome were obtained using thetaStat

794 do_stat. Sliding-window diversity profiles were then computed for each chromosome
795 with thetaStat do_stat -win 50000 -step 10000, producing 50 kb windows stepped every
796 10 kb.

797 Linkage mapping

798 **Phenotype bioassay**

799 A total of 395 F_2 intercross larvae were tested on fresh Bt soybean leaves expressing the
800 insecticidal protein Cry1Ac. Of these, 303 larvae survived (77%) and 92 larvae died (23%).
801 Following DNA extraction and library preparation, due to the low quality of some DNA
802 samples, we successfully sequenced 87 surviving larvae (58%) and 62 dead larvae (42%),
803 resulting in a total of 149 sequenced larvae from the F_2 intercross population.
804

805 **Linkage map**

806 The linkage map was constructed using Lep-MAP3 [31], utilizing genotypic data from 149 F_2
807 individuals along with their parents and grandparents, totalling 3,738 markers. The
808 "ParentCall2" module (with the option removeNonInformative=1) was employed to
809 estimate the most accurate posterior probabilities of parental genotypes. Additionally,
810 we used the "Filtering2" module (with the option dataTolerance=0.01) to remove markers
811 exhibiting significant segregation distortion. The modules "SeparateChromosomes2"
812 and "joinSingles2all" were not utilized because the reference genome is assembled at
813 the chromosome level; thus, markers were retained on their respective chromosomes.
814

815 We ran the "OrderMarker2" module for each of the 31 chromosomes 15 times and
816 selected the run with the highest likelihood score. In this step, specific options such as

“outputPhasedData=1”, “recombination2=0”, “usePhysical=1 0.1” and “useKosambi=1” were applied. The “OrderMarker2” module orders markers within each linkage group by maximizing the likelihood of the data given the marker order. Markers that did not show strong linkage with their flanking markers were manually removed to avoid long gaps. The final linkage map provided phased chromosomal marker data with missing genotypes imputed. The phased data were converted for QTL mapping using Lep-MAP3’s map2genotypes.awk script, and the genotypes 1 1, 1 2, 2 1, and 2 2 were transformed to AA, AB, AB, and BB, respectively.

The final linkage map consisted of 3,735 markers distributed across 31 linkage groups (LGs), covering a total length of 3,661.8 centimorgans (cM). The number of markers per LG ranged from 95 to 156, and LG lengths varied between 88.3 and 143.6 cM. The average inter-marker spacing within each LG ranged from 1.4 to 14.2 cM (Extended Data Fig. 30 and Table S2).

QTL Mapping

QTL mapping was performed using the R/qtl package [32] in the R program [33], employing the Expectation-Maximization (EM) algorithm implemented in the “scanone” function. The phenotypes “survival” and “death” were coded as “1” and “0”, respectively, and the parameter model = "binary" was specified to accommodate the binary nature of the trait. The functions “fitqtl” (with drop-one-term analysis) and, subsequently, “refineqtl” were used to identify QTL positions with maximum likelihood under a fixed QTL model. The significant LOD threshold (0.95 percentile) was determined through 10,000 permutation tests. Confidence intervals for the detected QTLs were estimated using the “lodint”

841 function. Additionally, we used the “scantwo” function to perform a two-dimensional
842 genome scan with a two-QTL model to detect potential epistatic interactions between
843 QTLs.
844
845 The QTL analysis for the survival trait revealed suggestive peaks (LOD > 4.09) (Extended
846 Data Table 3 and Fig. 1). Two significant QTLs associated with survival were identified,
847 one on LG 5 (LOD = 6.48, $P < 0.05$) and another on LG 12 (LOD = 8.80, $P = 0.004$)
848 (Extended Data Fig. 31). Additionally, a peak was observed on LG 12 at position 104.9 cM.
849 However, the QTL analysis did not support this peak (LOD = 0.51, $P = 0.303$). The QTL on
850 LG 5 exhibited a confidence interval of 15.18 cM, while the QTL on LG 12 had a
851 confidence interval of 9.65 cM (Extended DataTable 3).
852
853 An epistatic interaction test between the QTLs on LGs 5 and 12 showed no significant
854 interaction (LOD = 1.42, $P = 1$), indicating that these QTLs do not exhibit epistatic effects
855 associated with the survival trait (Extended Data Table 4). Individuals carrying the
856 heterozygous genotype of the QTL on LG 5 displayed intermediate survival, indicative of
857 incomplete dominance. In contrast, the survival was lowest among those with the
858 heterozygous genotype of the QTL on LG 12, suggesting underdominance (Extended Data
859 Figure 32 and Extended Data Table 5).
860
861 **Identification of Candidate genes**
862 To investigate potential genes associated with *H. armigera* survival in soybeans that
863 express Cry1Ac protein, we used a 300 kb upstream and downstream of regions near
864 each significant QTL marker identified. This process utilized the genome annotation file

(GCF_030705265.1-RS_2024_03) from *H. armigera* genome assembly GCF_030705265.1 published in the NCBI.

Data Availability

All newly generated sequencing data have been uploaded to the ENA: ERP162059.

Sample metadata is available in Table S1 and on the Earthcape database:

https://heliconius.ecdb.io/

Code Availability

Custom scripts available at https://github.com/Insect-evolution-and-genetics-lab/genome_collision_scripts

Methods References

1. G. T. Behere, W. T. Tay, D. A. Russell, P. Batterham, Molecular markers to discriminate among four pest species of Helicoverpa (Lepidoptera: Noctuidae). *Bull Entomol Res* 98, 599–603 (2008).
2. M. Kučka, Y. F. Chan, HMW DNA extraction using magnetic beads (2022)p. dx.doi.org/10.17504/protocols.io.b46bqzan.
3. J. J. Doyle, J. L. Doyle, A rapid DNA isolation procedure for small quantities of fresh leaf tissue. *PHYTOCHEMICAL BULLETIN* (1987).
4. S. Picelli, Å. K. Björklund, B. Reinius, S. Sagasser, G. Winberg, R. Sandberg, Tn5 transposase and tagmentation procedures for massively scaled sequencing projects. *Genome Res* 24, 2033–2040 (2014).
5. J. I. Meier, P. A. Salazar, M. Kučka, R. W. Davies, A. Dréau, I. Aldás, O. B. Power, N. J. Nadeau, J. R. Bridle, C. Rolian, N. H. Barton, W. O. McMillan, C. D. Jiggins, Y. F. Chan, Haplotype tagging reveals parallel formation of hybrid races in two butterfly species. *Proc Natl Acad Sci U S A* 118, e2015005118 (2021).
6. F. Mölder, K. P. Jablonski, B. Letcher, M. B. Hall, C. H. Tomkins-Tinch, V. Sochat, J. Forster, S. Lee, S. O. Twardziok, A. Kanitz, A. Wilm, M. Holtgrewe, S. Rahmann, S. Nahnsen, J. Köster, M. Reich, Sustainable data analysis with Snakemake. *F1000Research 2021 10:33* 10, 33 (2021).
7. M. Jin, H. L. North, Y. Peng, H. Liu, B. Liu, R. Pan, Y. Zhou, W. Zheng, K. Liu, B. Yang, L. Zhang, Q. Xu, S. Elfekih, W. A. Valencia-Montoya, T. Walsh, P. Cui, Y. Zhou, K. Wilson, C. Jiggins, K. Wu, Y. Xiao, Adaptive evolution to the natural and

anthropogenic environment in a global invasive crop pest, the cotton bollworm. *The Innovation* 4, 100454 (2023).

8. S. Chen, Y. Zhou, Y. Chen, J. Gu, fastp: an ultra-fast all-in-one FASTQ preprocessor. *Bioinformatics* 34, i884–i890 (2018).
9. H. Li, R. Durbin, Fast and accurate short read alignment with Burrows–Wheeler transform. *Bioinformatics* 25, 1754–1760 (2009).
10. H. Li, B. Handsaker, A. Wysoker, T. Fennell, J. Ruan, N. Homer, G. Marth, G. Abecasis, R. Durbin, The Sequence Alignment/Map format and SAMtools. *Bioinformatics* 25, 2078–2079 (2009).
11. Broad Institute, Picard toolkit, *GitHub repository* (2023). http://broadinstitute.github.io/picard/.
12. A. Orteu, M. Kucka, I. J. Gordon, I. Ng'iru, E. S. M. Van der Heijden, G. Talavera, I. A. Warren, S. Collins, R. H. Ffrench-Constant, D. J. Martins, Y. F. Chan, C. D. Jiggins, S. H. Martin, Transposable Element Insertions Are Associated with Batesian Mimicry in the Pantropical Butterfly Hypolimnas misippus. *Mol Biol Evol* 41 (2024).
13. G. A. Van der Auwera, M. O. Carneiro, C. Hartl, R. Poplin, G. del Angel, A. Levy-Moonshine, T. Jordan, K. Shakir, D. Roazen, J. Thibault, E. Banks, K. V. Garimella, D. Altshuler, S. Gabriel, M. A. DePristo, From FastQ Data to High-Confidence Variant Calls: The Genome Analysis Toolkit Best Practices Pipeline. *Curr Protoc Bioinformatics* 43, 11.10.1-11.10.33 (2013).
14. C. J. Anderson, J. G. Oakeshott, W. T. Tay, K. H. J. Gordon, A. Zwick, T. K. Walsh, Hybridization and gene flow in the mega-pest lineage of moth, Helicoverpa. *Proceedings of the National Academy of Sciences*, 201718831 (2018).
15. K. L. Taylor, K. A. Hamby, A. M. DeYonke, F. Gould, M. L. Fritz, Genome evolution in an agricultural pest following adoption of transgenic crops. *Proc Natl Acad Sci U S A* 118, e2020853118 (2021).
16. H. L. North, Z. Fu, R. Metz, M. A. Stull, C. D. Johnson, X. Shirley, K. Crumley, D. Reisig, D. L. Kerns, T. Gilligan, T. Walsh, C. D. Jiggins, G. A. Sword, Rapid Adaptation and Interspecific Introgression in the North American Crop Pest Helicoverpa zea. *Mol Biol Evol* 41 (2024).
17. W. A. Valencia-Montoya, S. Elfekih, H. L. North, J. I. Meier, I. A. Warren, W. T. Tay, K. H. J. Gordon, A. Specht, S. V. Paula-Moraes, R. Rane, T. K. Walsh, C. D. Jiggins, Adaptive Introgression across Semipermeable Species Boundaries between Local Helicoverpa zea and Invasive Helicoverpa armigera Moths. *Mol Biol Evol* 37, 2568–2583 (2020).
18. R. Guo, A. Papanicolaou, M. L. Fritz, Validation of reference-assisted assembly using existing and novel Heliothine genomes. *Genomics* 114, 110441 (2022).
19. Y. Xu, C. Wang, Z. Li, X. Zheng, Z. Kang, P. Lu, J. Zhang, P. Cao, Q. Chen, X. Liu, A chromosome-level haplotype-resolved genome assembly of oriental tobacco budworm (Helicoverpa assulta). *Sci Data* 11, 461- (2024).

20. J. Yin, G. Y. Hong, A. M. Wang, Y. Z. Cao, Z. J. Wei, Mitochondrial genome of the cotton bollworm Helicoverpa armigera (Lepidoptera: Noctuidae) and comparison with other Lepidopterans. *Mitochondrial DNA* 21, 160–169 (2010).
21. S. Liu, L. Zhang, Y. Sang, Q. Lai, X. Zhang, C. Jia, Z. Long, J. Wu, T. Ma, K. Mao, N. R. Street, P. K. Ingvarsson, J. Liu, J. Wang, Demographic History and Natural Selection Shape Patterns of Deleterious Mutation Load and Barriers to Introgression across Populus Genome. *Mol Biol Evol* 39 (2022).
22. B. M. Fitzpatrick, Estimating ancestry and heterozygosity of hybrids using molecular markers. *BMC Evol Biol* 12, 1–14 (2012).
23. M. Turelli, H. A. Orr, Dominance, epistasis and the genetics of postzygotic isolation. *Genetics* 154, 1663 (2000).
24. S. H. Martin, J. W. Davey, C. D. Jiggins, Evaluating the use of ABBA--BABA statistics to locate introgressed loci. *Mol Biol Evol* 32, 244–257 (2014).
25. H. Li, Minimap2: pairwise alignment for nucleotide sequences. *Bioinformatics* 34, 3094–3100 (2018).
26. F. Cabanettes, C. Klopp, D-GENIES: Dot plot large genomes in an interactive, efficient and simple way. *PeerJ* 2018, e4958 (2018).
27. K. W. Kim, R. De-Kayne, I. J. Gordon, K. S. Omufwoko, D. J. Martins, R. Ffrench-Constant, S. H. Martin, Stepwise evolution of a butterfly supergene via duplication and inversion. *Philos Trans R Soc Lond B Biol Sci* 377 (2022).
28. K. M. Benowitz, C. W. Allan, B. A. Degain, X. Li, J. A. Fabrick, B. E. Tabashnik, Y. Carriere, L. M. Matzkin, Novel genetic basis of resistance to Bt toxin Cry1Ac in Helicoverpa zea. *Genetics* 221 (2022).
29. A. R. Stahlke, J. Chang, L. R. Tembrock, S. B. Sim, S. Chudalayandi, S. M. Geib, B. E. Scheffler, O. P. Perera, T. M. Gilligan, A. K. Childers, K. J. Hackett, B. S. Coates, A Chromosome-Scale Genome Assembly of a Helicoverpa zea Strain Resistant to Bacillus thuringiensis Cry1Ac Insecticidal Protein. *Genome Biol Evol* 15 (2023).
30. S. L. Pearce, D. F. Clarke, P. D. East, S. Elfekih, K. H. J. Gordon, L. S. Jermiin, A. McGaughran, J. G. Oakeshott, A. Papanikolaou, O. P. Perera, others, Genomic innovations, transcriptional plasticity and gene loss underlying the evolution and divergence of two highly polyphagous and invasive Helicoverpa pest species. *BMC Biol* 15, 63 (2017).
31. P. Rastas, Lep-MAP3: robust linkage mapping even for low-coverage whole genome sequencing data. *Bioinformatics* 33, 3726–3732 (2017).
32. K. W. Broman, H. Wu, Ś. Sen, G. A. Churchill, R/qtl: QTL mapping in experimental crosses. *Bioinformatics* 19, 889–890 (2003).
33. R Core Team, R: A Language and Environment for Statistical Computing. R Foundation for Statistical Computing 4.2.1 [Preprint] (2022).
34. M. Jin, Y. Peng, J. Peng, S. Yu, C. Wu, X. Yang, J. Zhu, O. Infante, Q. Xu, H. Wang, K. Wu, Y. Xiao, A supergene controls facultative diapause in the crop pest Helicoverpa armigera. *Cell Rep* 43, 114939 (2024).

Acknowledgements

We are grateful to colleagues for their comments and feedback, especially Joana Meier and members of the Rapid Speciation Group at the Sanger Institute, and all members of the Insect Evolution and Genomics Group at Cambridge between 2019 and 2025. Jochen Wolf and Andrea Manica also provided thoughtful comments on preliminary results. HN was funded by the JS Gardiner Fund as a PhD student.

Author contributions

HLN: Conceptualisation (computational analysis, sampling design), data curation, formal analysis (bioinformatics), methodology (bioinformatics), project administration, software implementation, investigation (lab work). **GMK**: Conceptualisation (computational analysis, sampling design), data curation, formal analysis (bioinformatics), methodology (bioinformatics), project administration, software implementation, supervision (of AW), investigation (lab work). **DA**: Conceptualisation (computational analysis, experimental design), data curation, formal analysis (bioinformatics, linkage map), methodology development and implementation (DNA extraction and library preparation), project administration, investigation (bioassay), software implementation (QTL mapping), resources (sample provision). **IAW:** Methodology (DNA extraction and library preparation), investigation (lab work), data curation. **MK:** Methodology (DNA extraction, library preparation, haplotagging), investigation (lab work). **AW:** formal analysis (spatial analysis). **YFC:** Conceptualisation, Resources, Funding. **TW:** Conceptualisation, Resources, Funding, Data Curation. **ASC:** Conceptualisation, Investigation (DNA extraction and Library preparation), Formal Analysis (preliminary analysis), Resources, Funding, Data

Curation, Project Administration. **CO:** Conceptualisation, Resources, Funding, Data Curation, Project Administration. **CDJ:** Conceptualisation, Supervision (of HLN, GMK, DA, AW), Resources, Funding, Data Curation, Project Administration.

Competing Interests Declaration

The authors declare no competing interests.

Funding

This research was supported by BBSRC grant BB/V001329/1, the São Paulo Research Foundation (FAPESP), Brazil (process numbers: 2022/15206-2, 2020/00708-7, 2019/18282-9) and the National Council for Scientific and Technological Development (CNPq), Brazil (314160/2020-5).

Extended Data

Citations used in Extended Data Tables and Figures correspond to those in the Methods References.

Extended Data Table 2. Linkage map summary.

LG	Nº Marker	Length	Ave. Spacing	Max. Spacing
1	119	141.5	1.2	6.9
2	127	122.8	1.0	4.8
3	133	96.6	0.7	2.1
4	119	112.4	1.0	3.5
5	124	88.3	0.7	1.4
6	127	93.8	0.7	1.4
7	141	138.0	1.0	6.9
8	136	125.6	0.9	8.4
9	119	109.7	0.9	4.1
10	128	110.4	0.9	3.5
11	112	93.8	0.8	4.1
12	130	111.8	0.9	3.5
13	122	114.5	0.9	3.5
14	117	91.7	0.8	3.5
15	130	143.6	1.1	6.2
16	125	135.3	1.1	5.5
17	116	97.3	0.8	2.8
18	117	115.9	1.0	4.8
19	156	141.4	0.9	2.8
20	137	142.8	1.1	3.5
21	121	127.0	1.1	5.5
22	121	111.1	0.9	3.5
23	110	95.9	0.9	3.5
24	110	137.4	1.3	5.5
25	101	120.8	1.2	6.2
26	112	104.9	0.9	4.8
27	98	133.3	1.4	5.5
28	119	125.6	1.1	4.8
29	100	123.6	1.2	6.2
30	95	130.1	1.4	14.2
31	113	125.0	1.1	7.6
Overall	**3,735**	**3,661.8**	**-**	**-**

Extended Data 3. Localisation and LOD scores of markers in the QTL peak and confidence intervals for Cry1Ac resistance in the *Helicoverpa armigera* F2 intercross population.

QTL	LG	Pos (cM)	LOD	*P*	Low Pos (cM)	High Pos (cM)
Q1	5	62.76	6.48	3.29×10^{-07}	51.72	66.90
Q2	12	2.76	8.80	1.57×10^{-09}	0.69	10.34

Extended Data 4. Summary table of the two-QTL genome scan to identify QTL interactions between the QTL involved in survival trait in *H. armigera* resistant to Cry1Ac.

LG	Pos (cM)	LG	Pos (cM)	LOD Full[a]	*P*	LOD FV[b]	*P*	LOD Int.[c]	*P*	LOD Add.[d]	*P*	LOD AV[e]	*P*
5	62.76	12	2.76	14.77	< 0.05	7.90	< 0.05	1.42	1	13.35	< 0.05	6.48	< 0.05

[a]LOD Full: The LOD score of the full model encompasses both QTLs and their interaction.
[b]LOD FV: The LOD score of the full model compared to a model that includes only the second QTL (Pos2) without the first QTL (Pos1).
[c]LOD Int: The LOD score for the interaction between the two QTLs.
[d]LOD Add: The LOD score of the additive model that includes both QTLs without considering their interaction.
[e]LOD AV: The LOD score of the additive model compared to a model that includes only the second QTL (Pos2) without the first QTL (Pos1).

Extended Data 5. Genotypic frequencies of markers identified at QTL peaks associated with *Helicoverpa armigera* survival to the Cry1Ac protein.

Genotype	Survival	Dead	Total	% Survival	% Dead
		QTL 1 - Marker rs5P9830222			
AA	38	12	50	76	24
AB	40	26	66	61	39
BB	7	22	29	24	76
Total	85	60	145		
		QTL 2 - Marker rs12P7798483			
AA	76	31	107	71	29
AB	2	19	21	10	90
BB	7	10	17	41	59
Total	85	60	145		

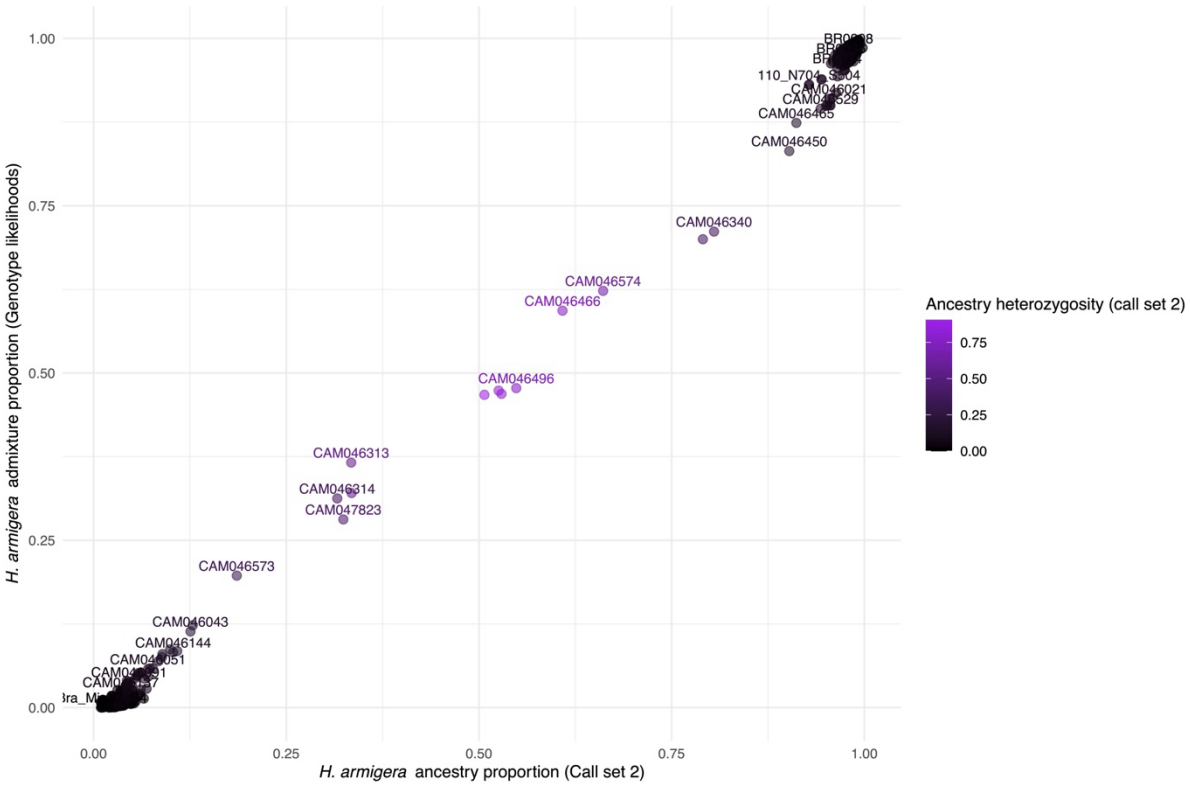

Extended Data Figure 1 *H. armigera* ancestry proportion (AP) calculated using genotype calls and reference non-admixed *H. armigera* and *h. zea* (horizontal axis) against the ancestry proportion calculated using genotype likelihoods (vertical axis), with individual sample IDs labelled. Points and text are coloured by the ancestry heterozygosity calculated using genotype calls, which is maximised in early-generation hybrids (Figure 1).

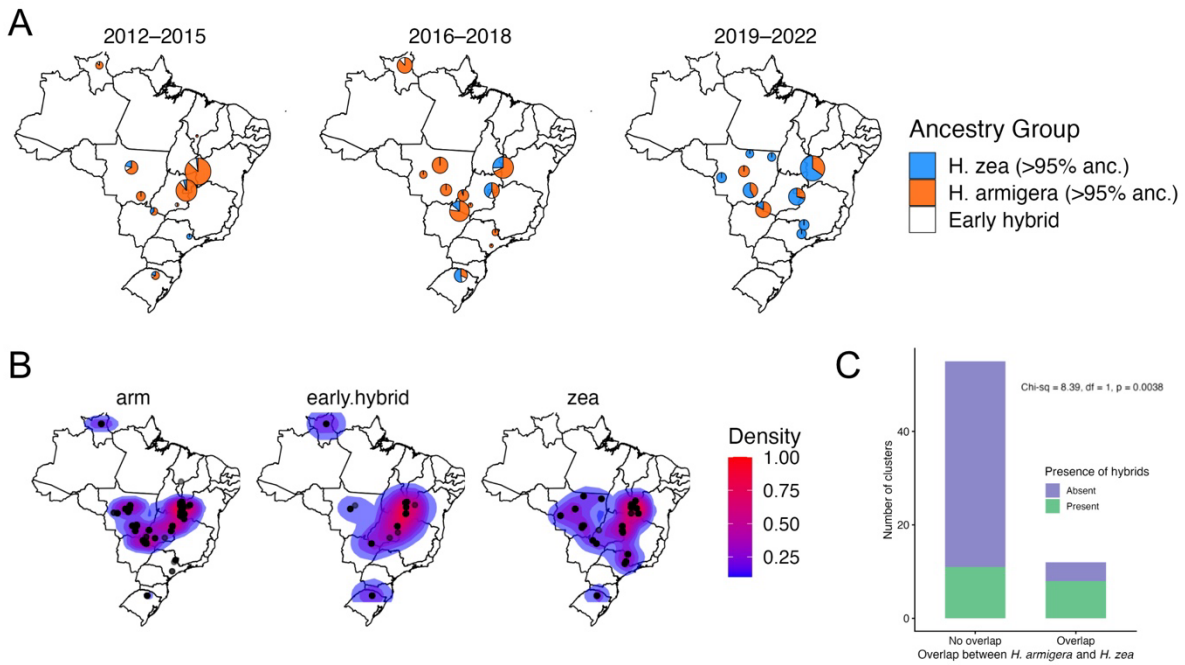

Extended Data Figure 2: Spatial and temporal dynamics of Helicoverpa ancestry and early-generation hybrid occurrence in Brazil. **(A)** Proportion of individuals assigned to >95% H. armigera ancestry (orange), >95% H. zea ancestry (blue), or early generation hybrids (white) across Brazilian sampling sites grouped into three time periods: 2012–2015, 2016–2018, and 2019–2022 and in clusters whereby individuals are at a maximum of 100 km from each other. Pie chart size is proportional to sample size per locality. **(B)** Kernel density distributions showing spatial clustering of H. armigera, early hybrids, and H. zea across Brazil. Warmer colours indicate higher density of sampled individuals. **(C)** Proportion of sampling clusters where early hybrids are present or absent, split by regions with spatial overlap vs no spatial overlap of the two parental species. Hybrids are significantly more common in regions where the distributions of H. armigera and H. zea overlap (Chi–sq = 8.39, df = 1, p = 0.0038).

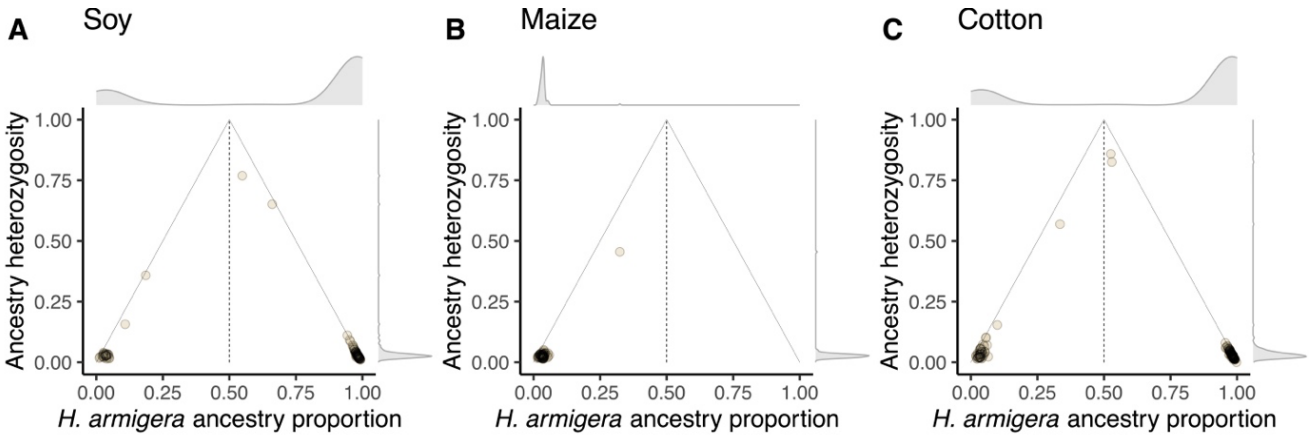

Extended Data Figure 3 Individual ancestry proportion (AP) and ancestry heterozygosity (AH) across all timepoints and sample sites as for Figure 1C, for each crop from which individuals were sampled: maize, cotton, soybean (A-C respectively). Predominantly-*H. armigera* samples were collected on soybean and cotton, while predominantly-*H. zea* samples were collected on maize.

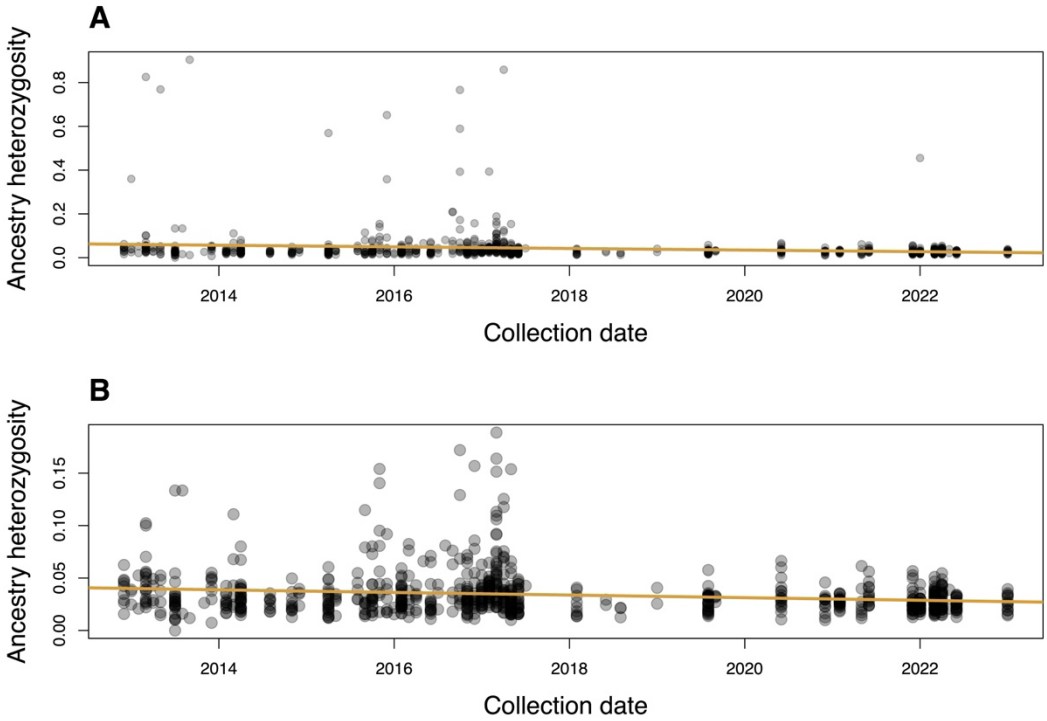

Extended Data Figure 4 Individual ancestry heterozygosity vs collection date. Line shows a fitted linear model, which has a significantly negative gradient (Person's product moment correlation: $p<0.01$, t = -4.9656, df = 746; correlation coefficient -0.177). **A**: all data shown. **B**: data shown for AH values <0.2.

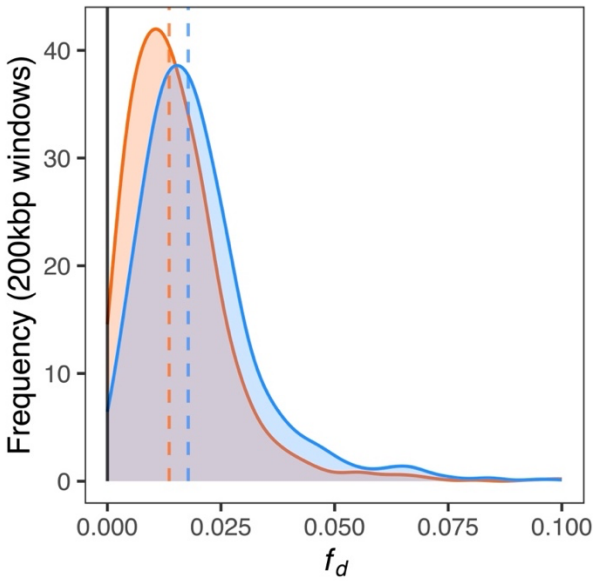

Extended Data Figure 5: Distribution of f_d calculated in 200kbp windows (horizontal axis limited to values between 0 and 0.1). Orange: gene flow from *H. armigera* to *H. zea* using the topology (((ZEA, ZEA_BRAZIL), ARM)), PUN); blue: gene flow from *H. zea* to *H. armigera* using the topology (((ARM, ARM_BRAZIL), ZEA)), PUN). Dashed lines indicate genome-wide medians: 0.0136 (*H. armigera* → *H. zea*), 0.0178 (*H. zea* → *H. armigera*).

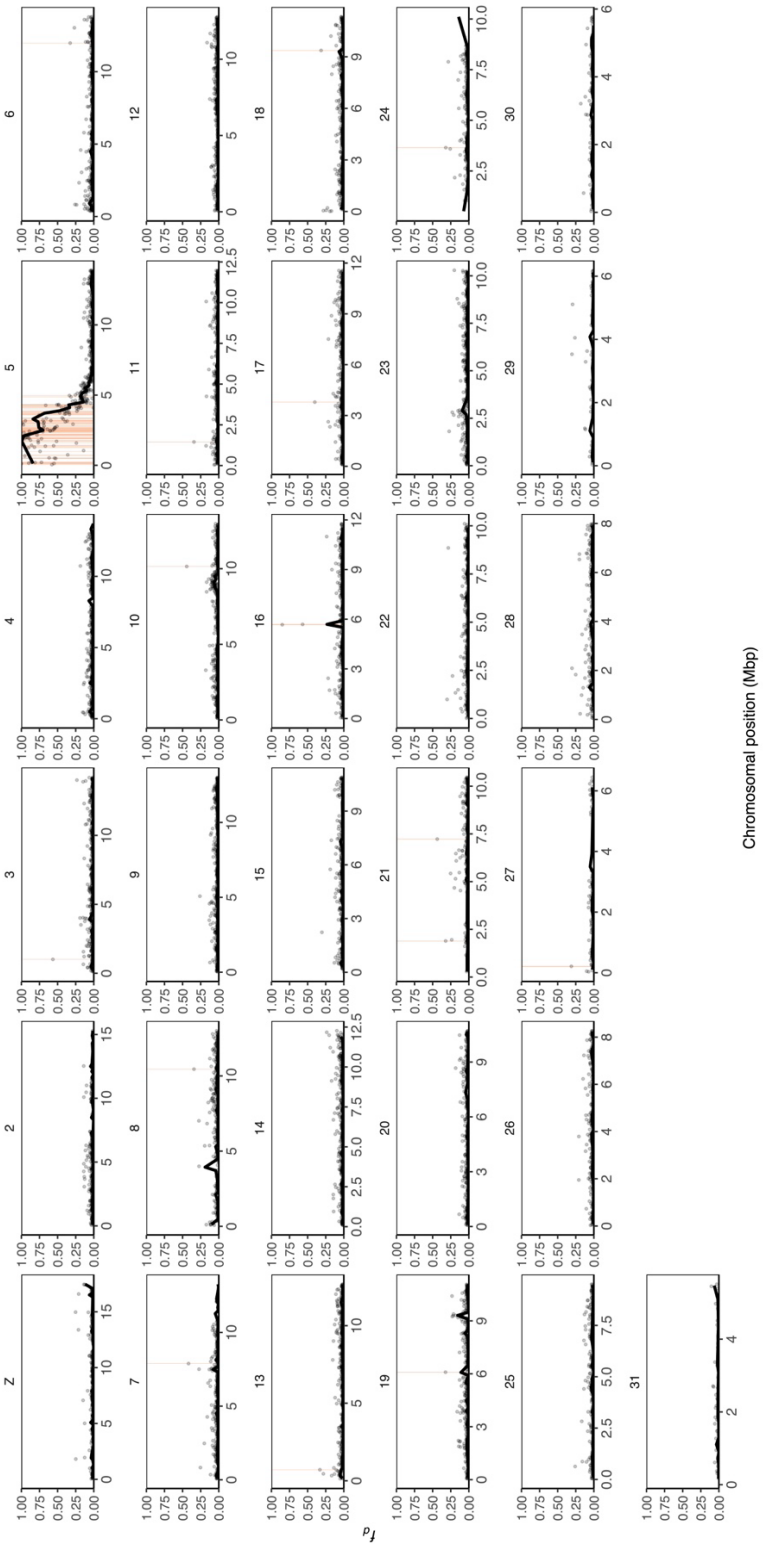

Extended Data Figure 6: Genome-wide landscape of introgression from *H. armigera* to *H. zea* across all timepoints and locations. f_d calculated in 200kbp windows (lines) and 20kbp windows (points) using the topology (((ZEA, ZEA_BRAZIL), ARM)), PUN). Highlighted windows indicate 20bkp windows in the upper first percentile of f_d values (those equal to or greater than 0.310).

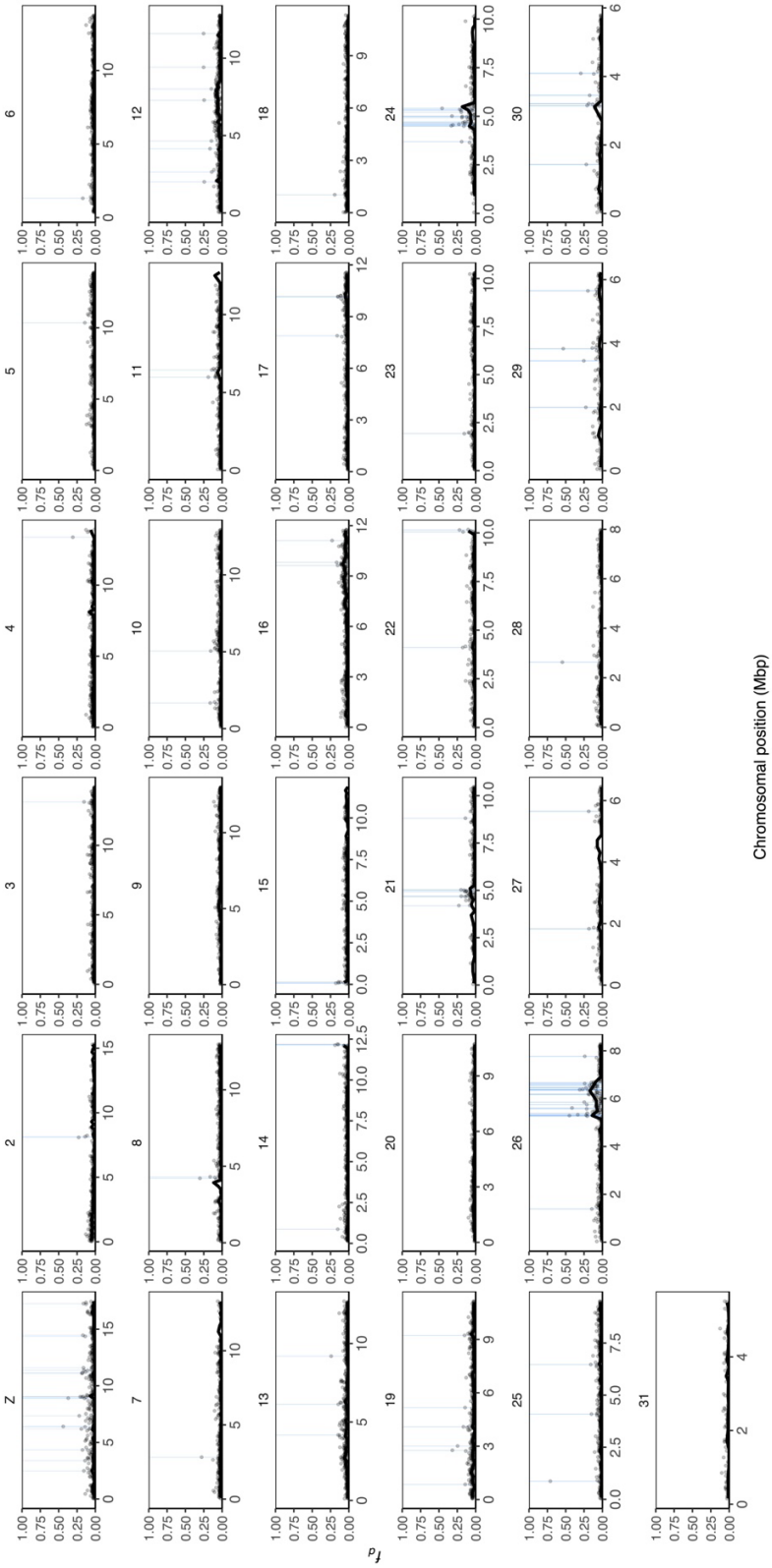

Extended Data Figure 7: Genome-wide landscape of introgression from *H. zea* to *H. armigera* across all timepoints and locations. f_d calculated in 200kbp windows (lines) and 20kbp windows (points) using the topology (((ZEA, ZEA_BRAZIL), ARM)), PUN). Highlighted windows indicate 20bkp windows in the upper first percentile of f_d values (those equal to or greater than 0.139).

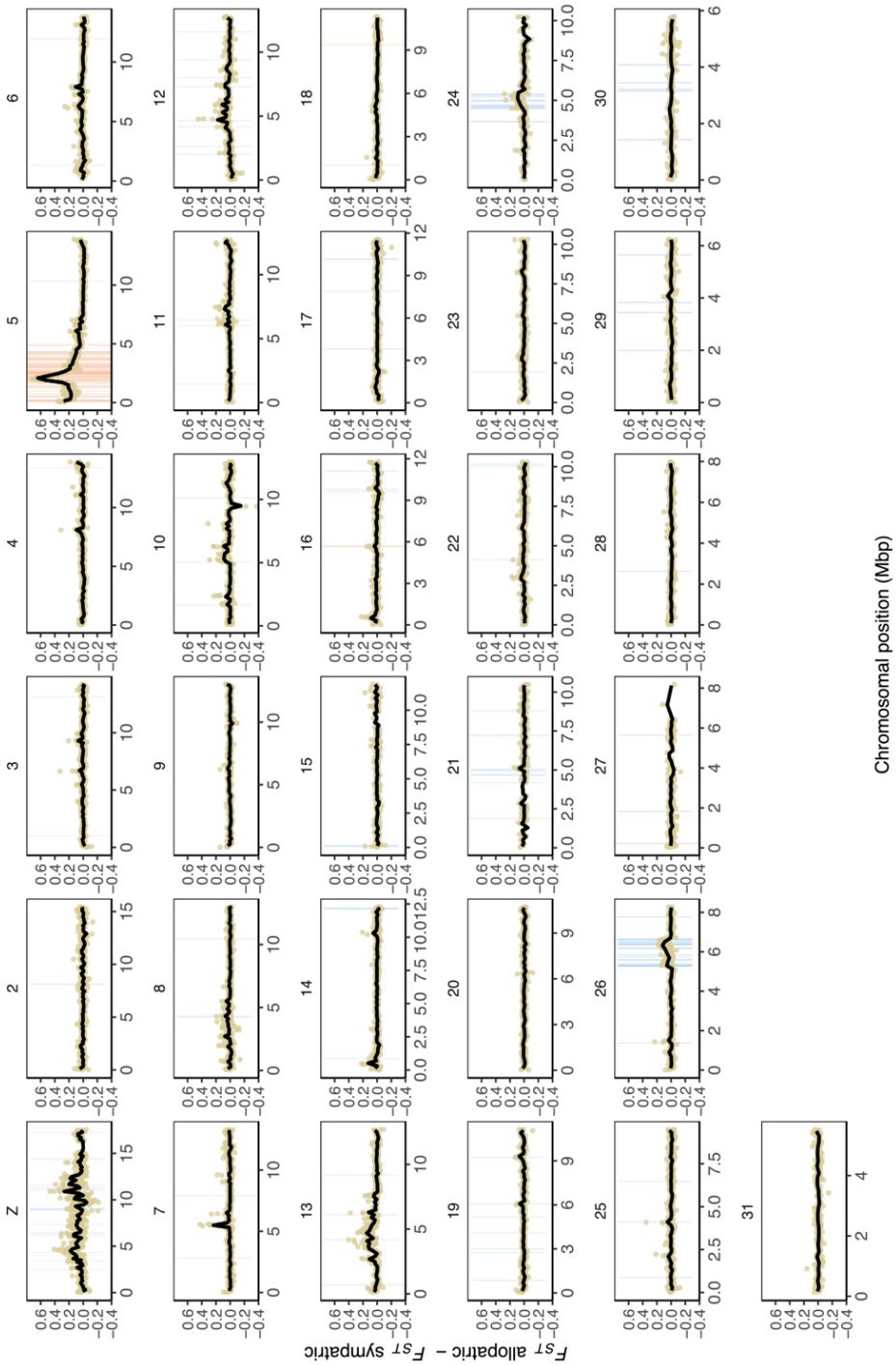

Extended Data Figure 8: Local reductions in genetic differentiation in sympatry relative to allopatry, between *H. armigera* and *H. zea*. Genetic differentiation (F_{ST}) was calculated in 200kbp windows with at least 500 informative sites (black lines) and 20kbp windows with at least 200 usable sites (points). "Allopatric" refers to the comparison of reference non-admixed *H. armigera* and *H. zea* in China and the United States respectively. "Sympatric" refers to the comparison of predominantly-*H. armigera* and predominantly-*H. zea* samples in Brazil, as defined by their ancestry proportion. Shaded regions indicate 20kbp windows with f_d values in the upper first percentile (blue: *H. zea* → *H. armigera*; orange: *H. armigera* → *H. zea*).

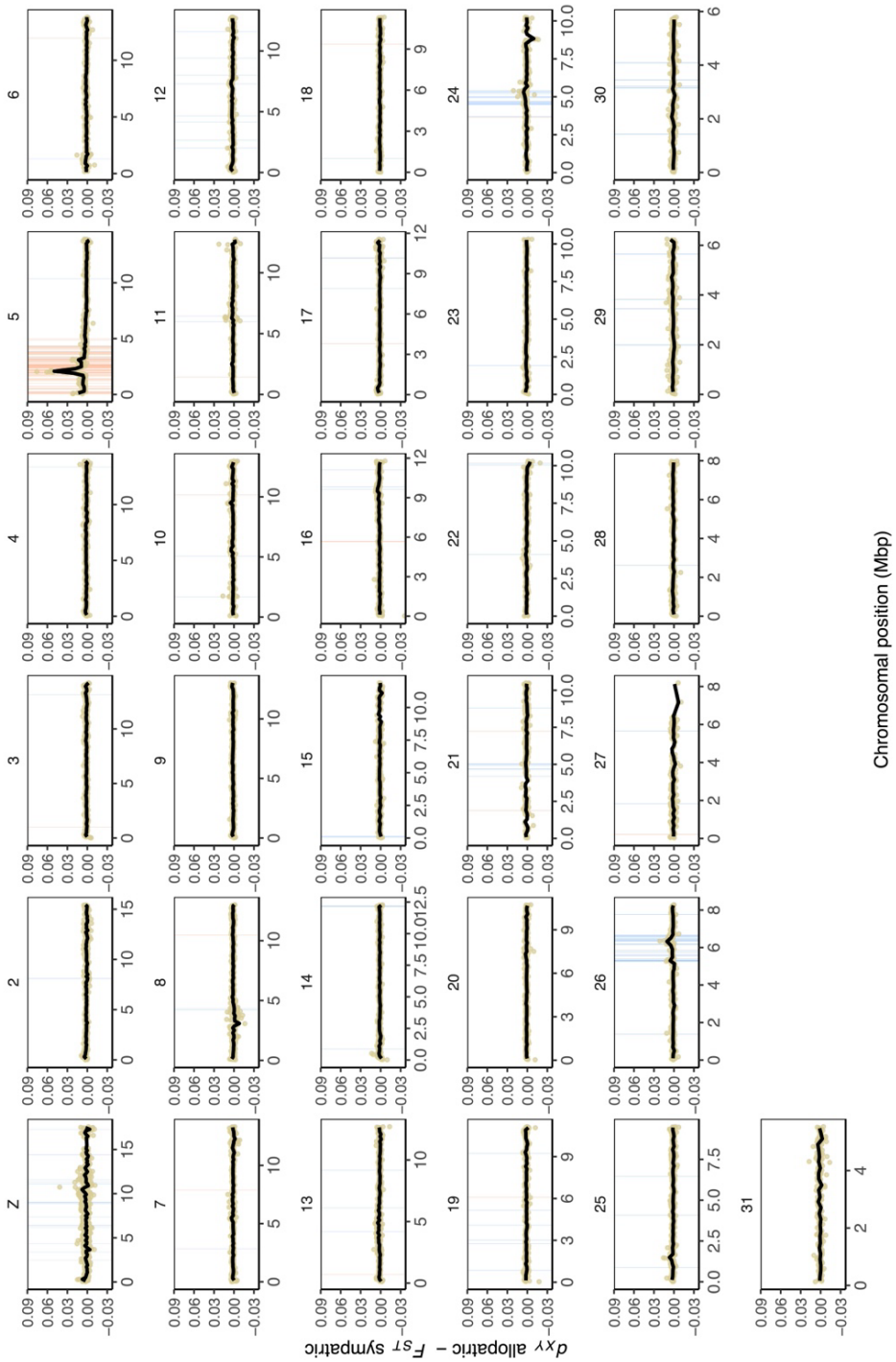

Extended Data Figure 9: Local reductions in genetic divergence in sympatry relative to allopatry, between *H. armigera* and *H. zea*. Genetic divergence (d_{XY}) was calculated in 200kbp windows with at least 500 informative sites (black lines) and 20kbp windows with at least 200 usable sites (points). "Allopatric" refers to the comparison of reference non-admixed *H. armigera* and *H. zea* in China and the United States respectively. "Sympatric" refers to the comparison of predominantly-*H. armigera* and predominantly-*H. zea* samples in Brazil, as defined by their ancestry proportion. Shaded regions indicate 20kbp windows with f_d values in the upper first percentile (blue: *H. zea* → *H. armigera*; orange: *H. armigera* → *H. zea*).

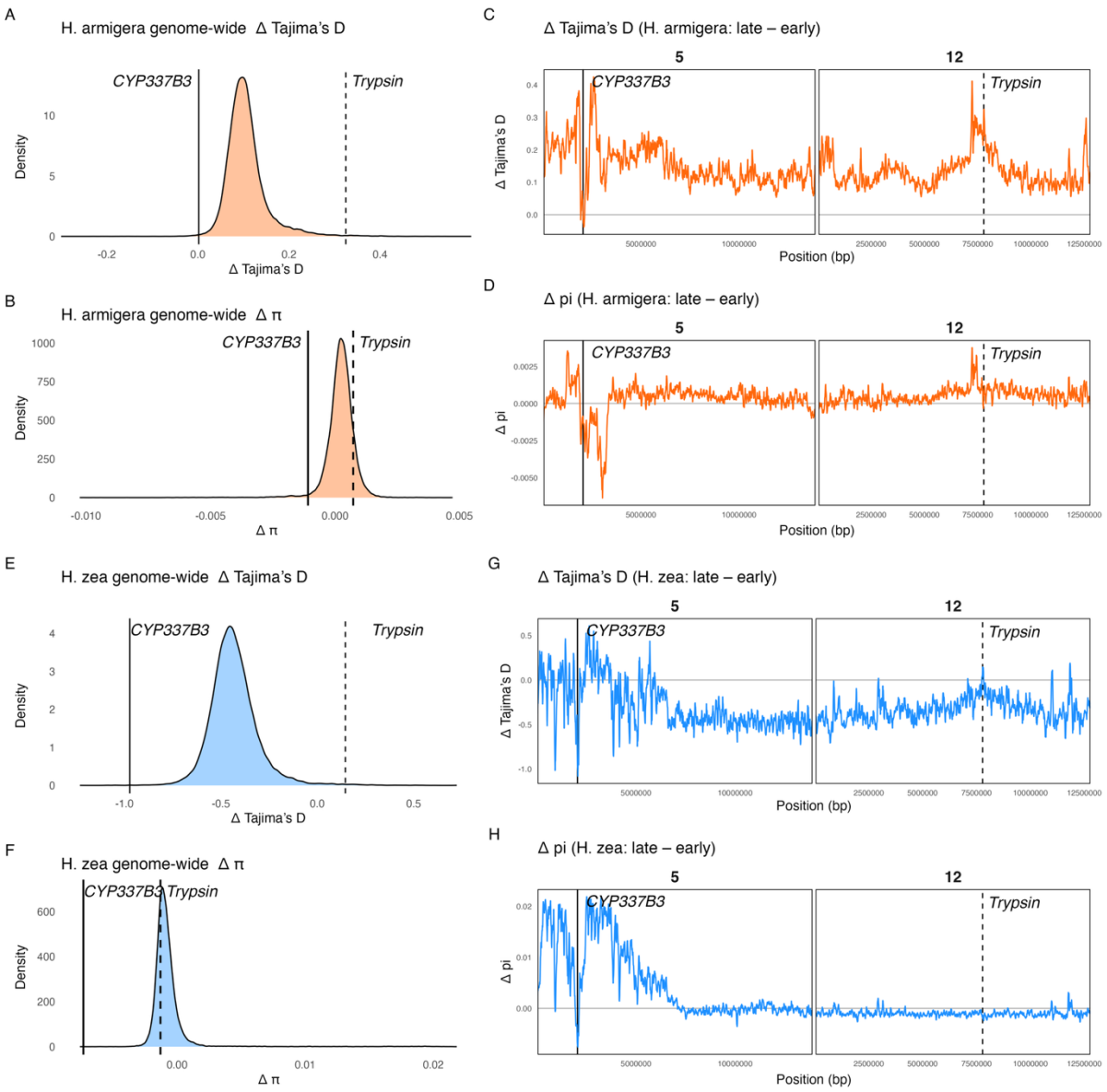

Extended Data Figure 10: Genome-wide and locus-specific shifts in diversity statistics calculated with ANGSD between early and late collections of *Helicoverpa armigera* (A-D) and *H. zea* (E-H). (A, B) Genome-wide distributions of ΔTajima's D (A, E) and Δπ (B, F) for *H. armigera* and *H. zea*, respectively (2012–2015 → 2019–2022). Vertical lines indicate the Δ values at CYP337B3 on chromosome 5 (solid) and the trypsin cluster on chromosome 12 (dashed). Chromosome-specific ΔTajima's D (C, G) and Δπ (D, H) across chromosomes 5 and 12 in *H. armigera* and *H. zea*, with the positions of CYP337B3 and the trypsin cluster marked.

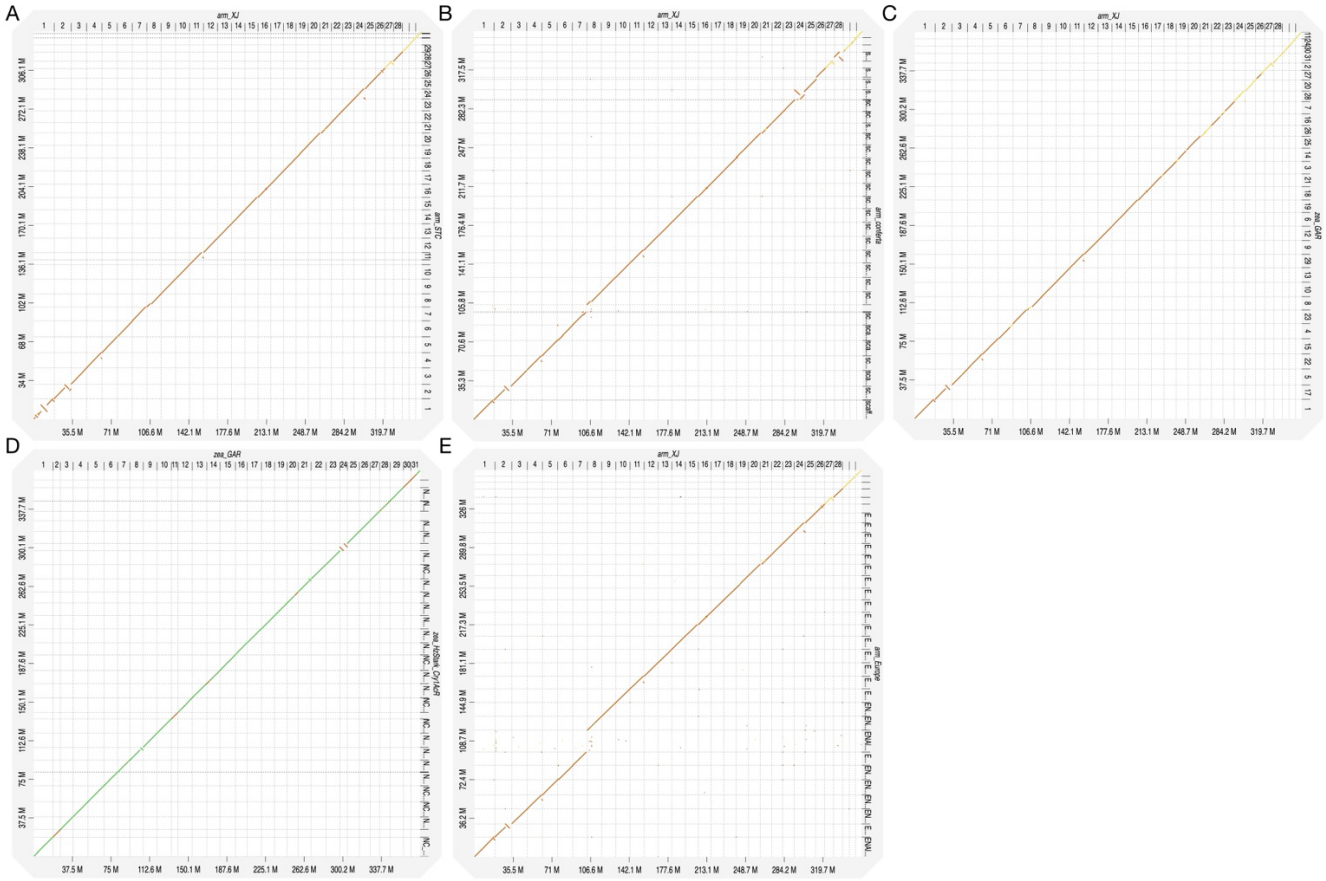

Extended Data Figure 11: Synteny is generally highly conserved within and between *Helicoverpa armigera* and *Helicoverpa zea*. Axes show scaffold positions of all 31 homologous chromosomes, where "1" corresponds to the Z chromosome in the arm_XJ reference genome used here. Grid lines delineate scaffolds. Colour corresponds to genetic divergence (green=low, yellow=medium, orange=high). **(A)** Comparison of the reference genome used here, derived from a sample collected in north-western China (horizontal axis) and a reference genome of a sample collected from a distinct *H. armigera* population in southern China (vertical axis) [34] **(B)** Comparison of the *H. armigera* reference genome used here (horizontal axis) and a reference genome generated for *H. armigera conferta*, collected in Australia (vertical axis) [29]. **(C)** Comparison of the *H. armigera* reference genome used here (horizontal axis) and the *H. zea* reference genome generated using the GA-R strain (vertical axis) [27]. **(D)** Comparison of the *H. zea* GA-R reference genome (vertical axis) and the *H. zea* HzStark_Cry1AcR strain [28]. **(E)** Comparison of the *H. armigera* reference genome used here (horizontal axis) and a *H. armigera* reference genome generated using a sample collected in Europe (vertical axis) [30].

H. zea strain HzStark_Cry1AcR

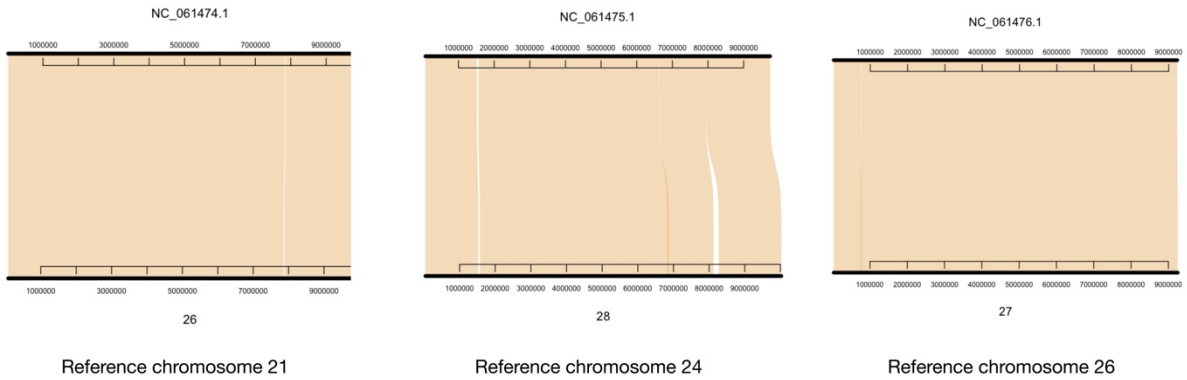

H. zea strain GA-R

Extended Data Figure 12: No inversion polymorphism between *H. zea* reference assemblies at the three chromosomes of interest. GA-R chromosomes 26, 28 and 27 correspond to chromosomes 21, 24 and 26 in the reference genome used here. Shaded regions show nucleotide alignments between the GA-R reference genome (lower scaffolds) [27] and the *H. zea* HzStark_Cry1AcR strain (upper scaffolds) [28].

H. armigera armigera (South China)

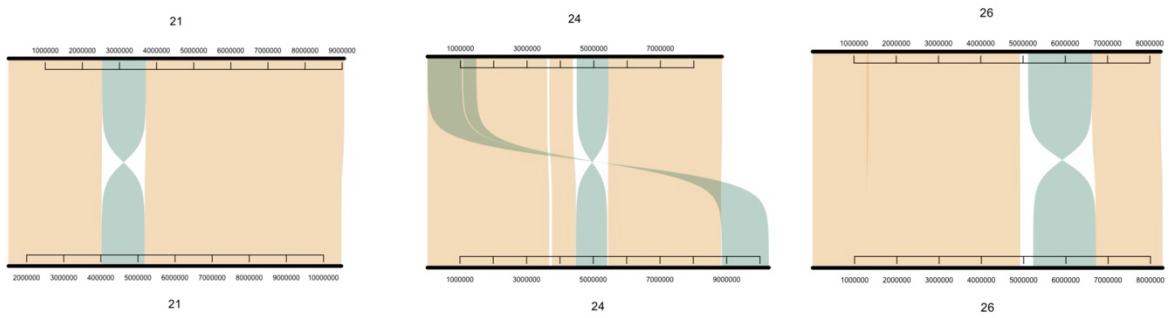

H. armigera armigera (Xinjiang)
Reference genome used here

Extended Data Figure 13: Inversions polymorphic between *H. armigera* and *H. zea* are also polymorphic between distinct *H. armigera* lineages. Shaded regions show nucleotide alignments between the reference genome used here (lower scaffolds) and a reference assembly generated from a sample collected in South China (upper scaffolds) [34].

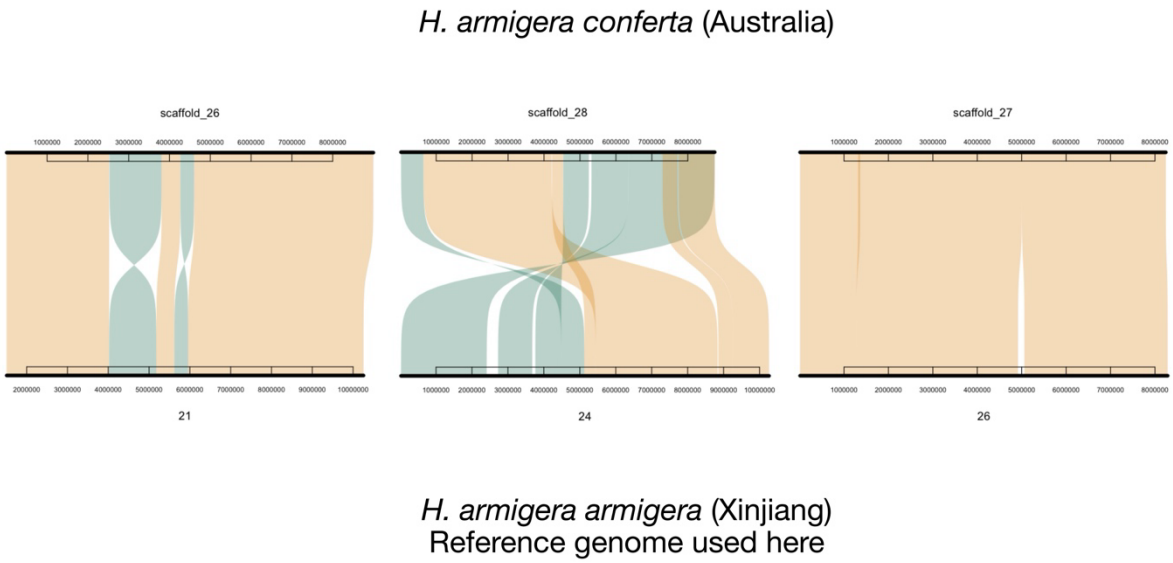

Extended Data Figure 14: On chromosome 26, inversions polymorphic between *H. armigera* and *H. zea* are not polymorphic between *H. armigera armigera* and *H. armigera conferta*. The other two inversions of interest are polymorphic within *H. armigera*. Shaded regions show nucleotide alignments between the reference genome used here (lower scaffolds) and a *H. armigera conferta* reference assembly [29].

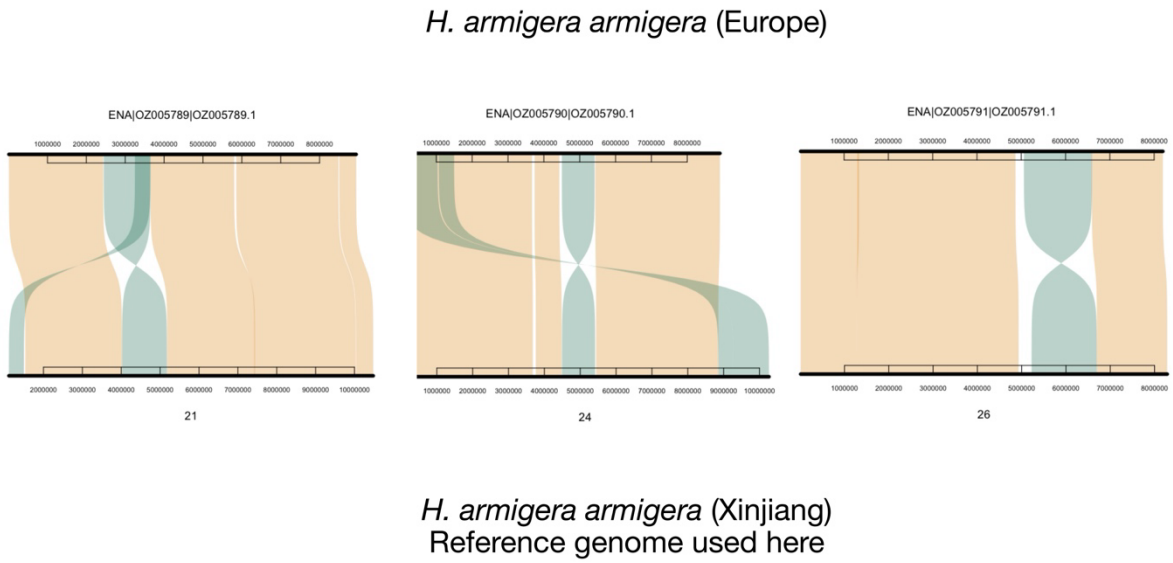

Extended Data Figure 15: Inversions polymorphic between *H. armigera* and *H. zea* are also polymorphic between *H. armigera* populations. Shaded regions show nucleotide alignments between the reference genome used here (lower scaffolds) and a reference assembly generated from a sample collected in Europe (upper scaffolds) [30]

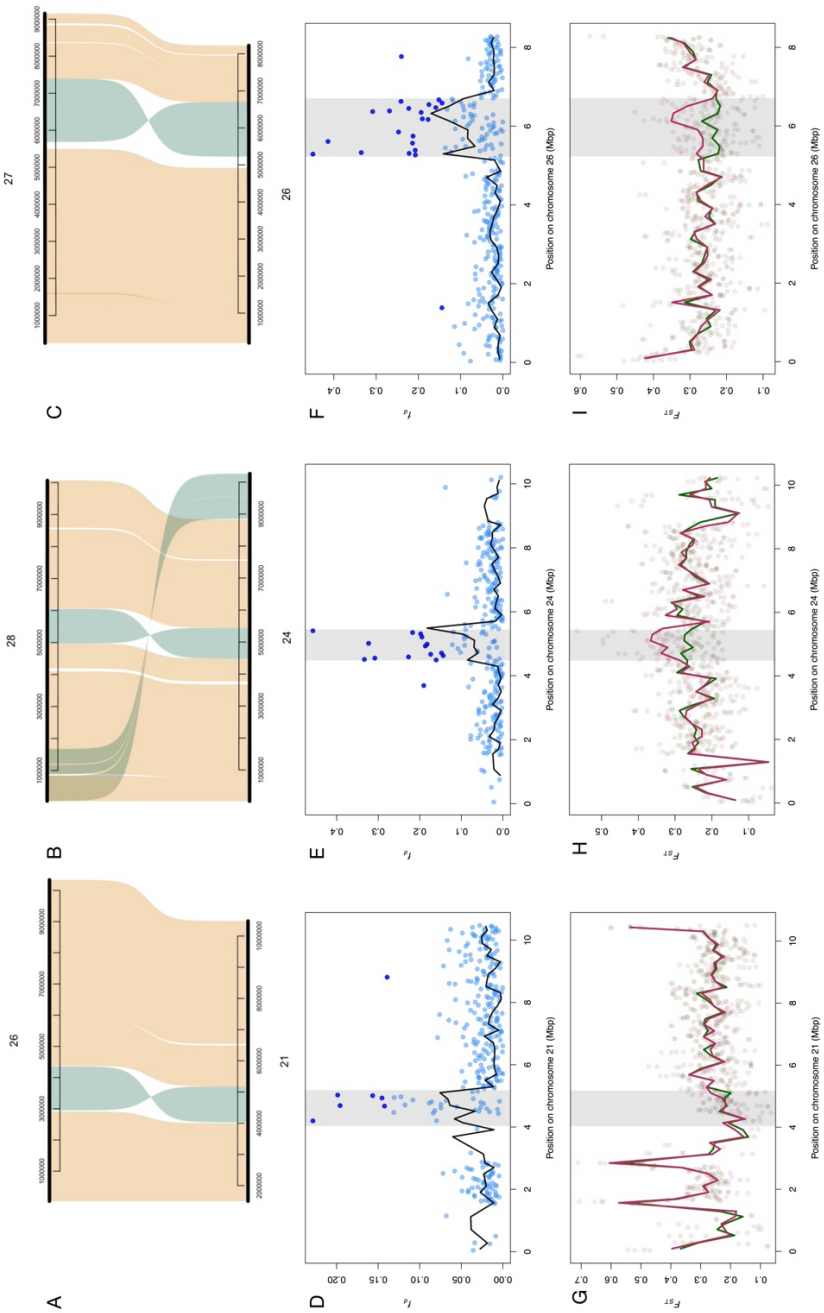

Extended Data Figure 16: Introgression of three *H. zea* inversions into *H. armigera*. All three inversions arose within *H. armigera*, so the introgressed *H. zea* haplotype is the ancestral orientation. **(A-C)** Synteny maps comparing the *H. armigera* reference genome used here (bottom scaffold) to the *H. zea* GA-R reference genome [27] for chromosomes 21, 24 and 26 respectively. Scaffold numbers indicate homologous chromosomes in the two assemblies (upper: *H. zea*, lower: *H. armigera*). **(D-F)** f_d (*H. zea* → *H. armigera*) calculated in non-overlapping 200kbp windows (lines) and 20kbp non-overlapping windows (points). Dark coloured points indicate those in the upper first percentile of f_d values genome-wide. Shaded regions indicate the bounds of the inversion identified in A. **(G-I)** F_{ST} calculated between allopatric non-admixed *H. armigera* and *H. zea* (maroon) and sympatric Brazilian *H. armigera* and *H. zea* (green). Lines: 200kbp windows, points: 20kbp windows.

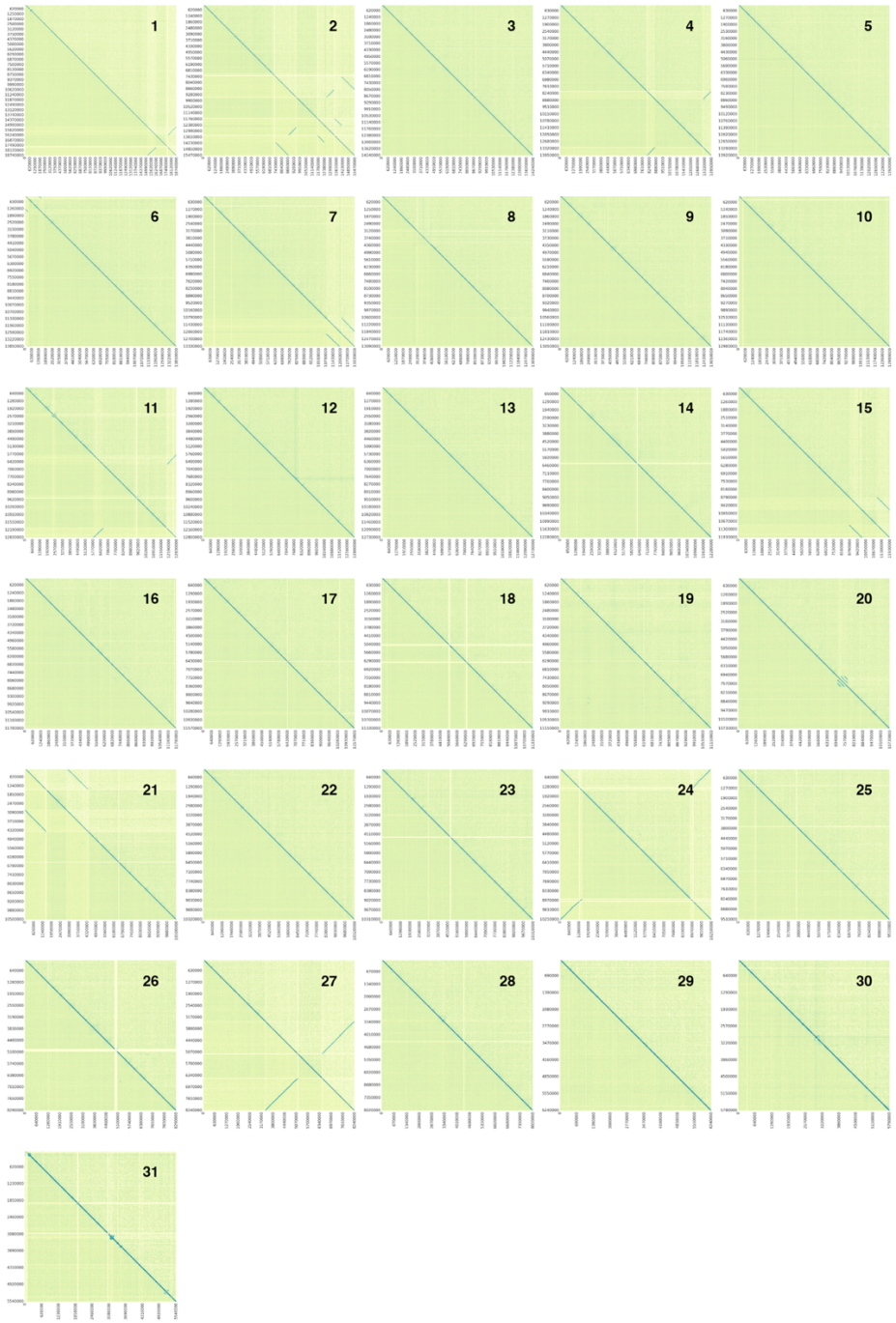

Extended Data Figure 17: Genome-wide barcode-sharing heatmaps used to detect structural variants in *H. zea* and *H. armigera*. Heatmaps show Wrath-derived barcode-sharing matrices across all chromosomes, calculated from linked-read BAM files using 10-kb non-overlapping windows. For each chromosome, the upper triangular matrix represents the *H. zea* dataset and the lower triangular matrix represents the *H. armigera* dataset. Colours reflect the Jaccard index of shared barcodes between window pairs, with darker regions indicating stronger barcode similarity. This method captures local deviations from the expected decay of barcode sharing with distance and highlights putative structural variants. Chromosome numbers are displayed in the upper right of each panel. Heatmaps correspond to the same matrices used by Wrath's SV-calling module (–l), which applies z-score outlier detection and a double exponential decay model to identify structural rearrangements.

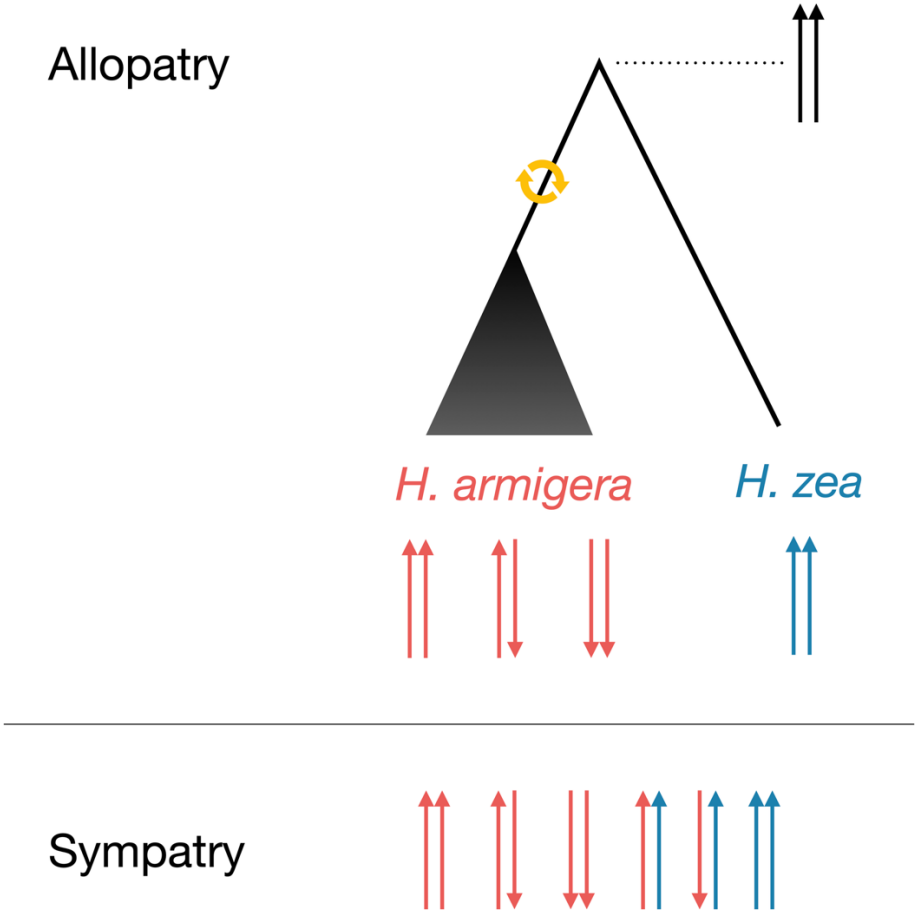

Extended Data Figure 18: Proposed scenario for all three inversion polymorphisms on chromosomes 21, 24 and 26, based on the most parsimonious explanation for inversion polymorphisms. An inversion mutation occurred within *H. armigera*, resulting in a derived inverted allele that remains polymorphic across divergent *H. armigera* lineages. The mutation occurred in a population ancestral to multiple present-day *H. armigera* lineages, or arose in one *H. armigera* lineage and spread to others. There are therefore three possible genotypes in allopatric *H. armigera* and one possible genotype in allopatric *H. zea*. Upon secondary sympatry in Brazil, there are six possible genotypes. Based on the available data I cannot exclude the possibility that the inversion was present in the ancestor to *H. armigera* and *H. zea*, but was lost in *H. zea*.

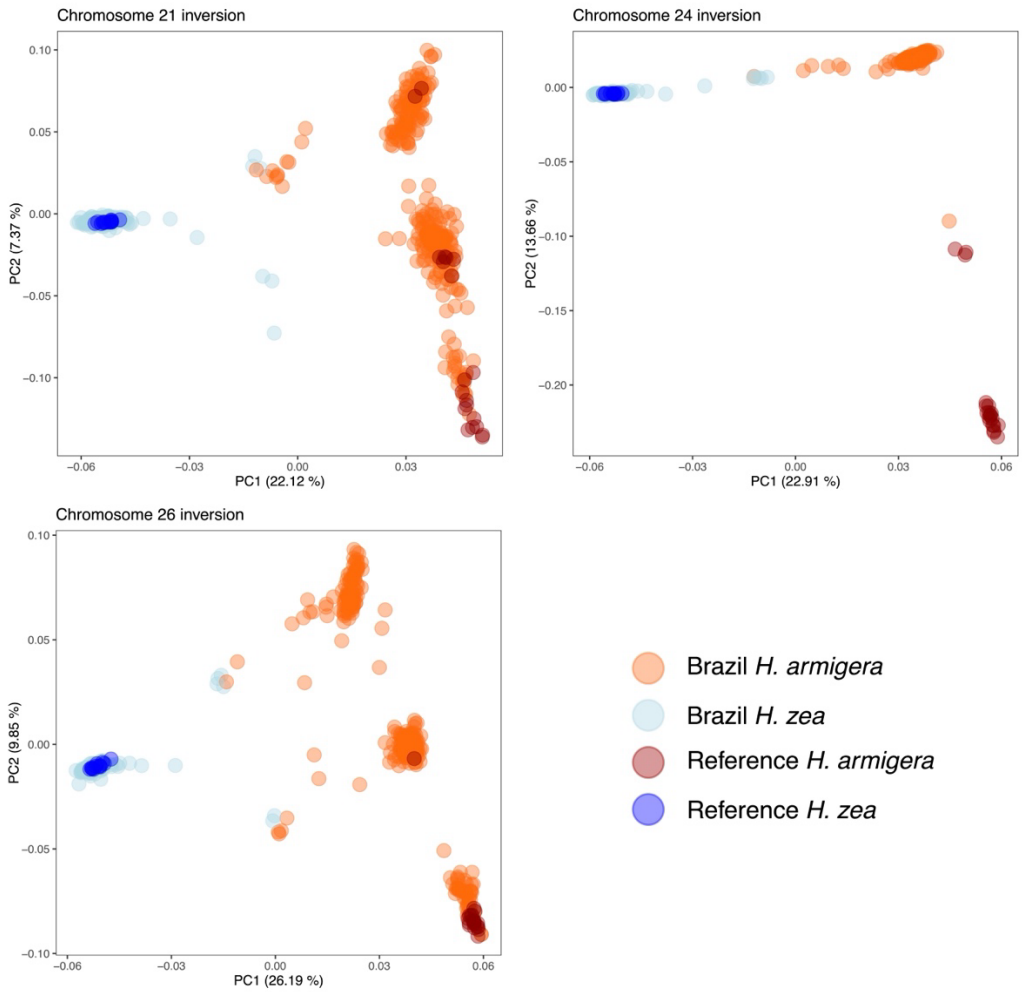

Extended Data Figure 19: PCA in in inversion regions confirms introgression from *H. zea* to *H. armigera*. Point colour corresponds to ancestry, as defined by the likelihood-based ancestry proportion. Unlike the pattern outside of inverted regions in which individuals cluster by ancestry proportion, in inversion regions individuals fall into three major clusters with up three rarer intermediate clusters. This is consistent with expectations under the proposed evolutionary scenario for all three inversions (Extended Data Fig. 18). Heterozygous individuals are overwhelmingly *H. armigera* samples, consistent with the introgression signal.

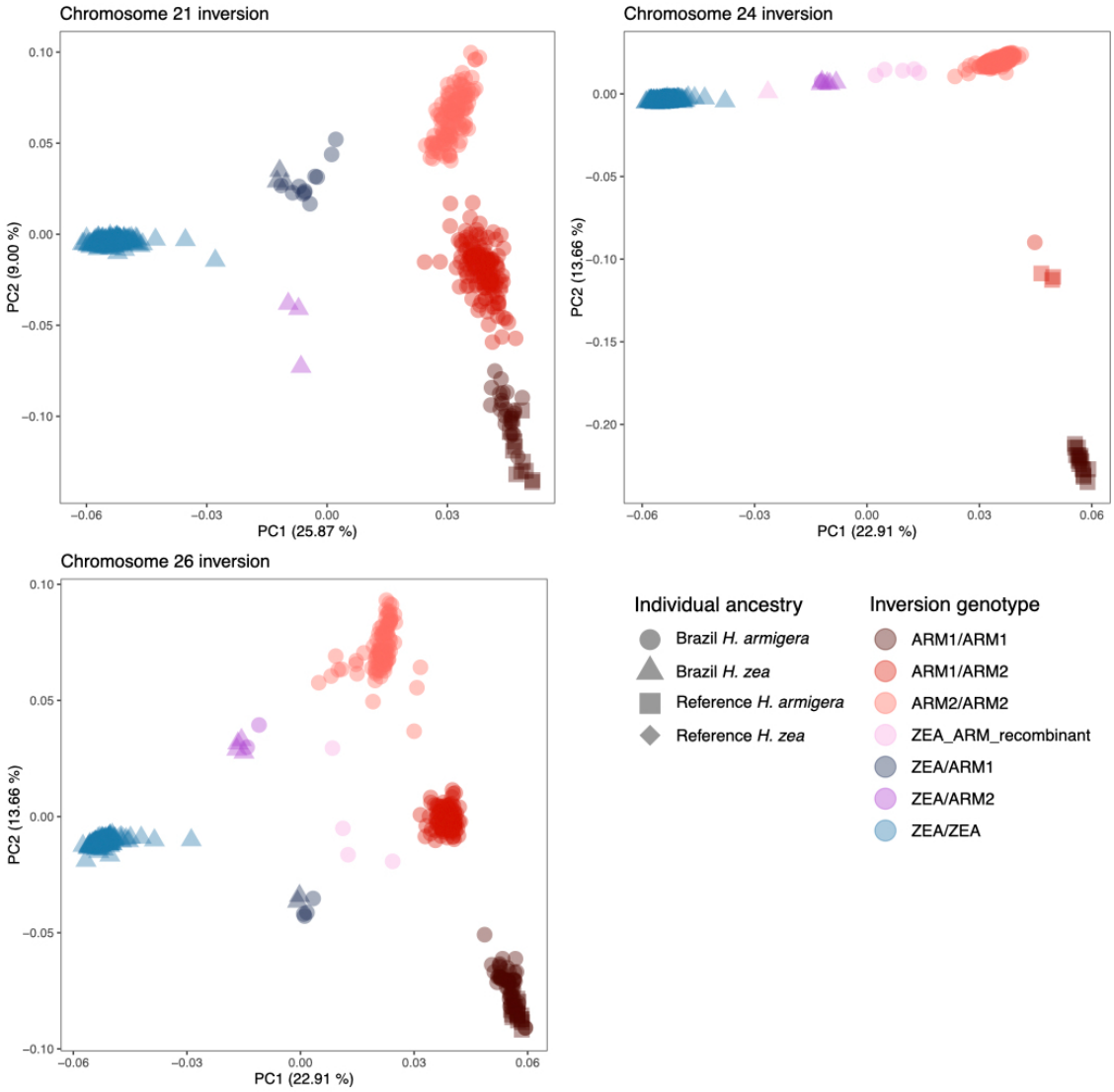

Extended Data Figure 20: Putative inversion genotypes assigned using PCA clusters. Shape corresponds to ancestry, colour corresponds to genotype assignment. This approach distinguishes between two possible *H. armigera* alleles, but does not assign which is ancestral or derived. This is because of the significant degree of genetic differentiation between the three putative homozygous genotypes. Unlike the pattern outside of inverted regions in which individuals cluster by ancestry proportion, in inversion regions individuals fall into three major clusters with up three rarer intermediate clusters. This fits expectations under the proposed evolutionary scenario for all three inversions. Individual genotype assignments are reported in Extended Data Table 1. Recombinant genotype assignments fall between genotype categories, representing possible cases of recombination or gene conversion.

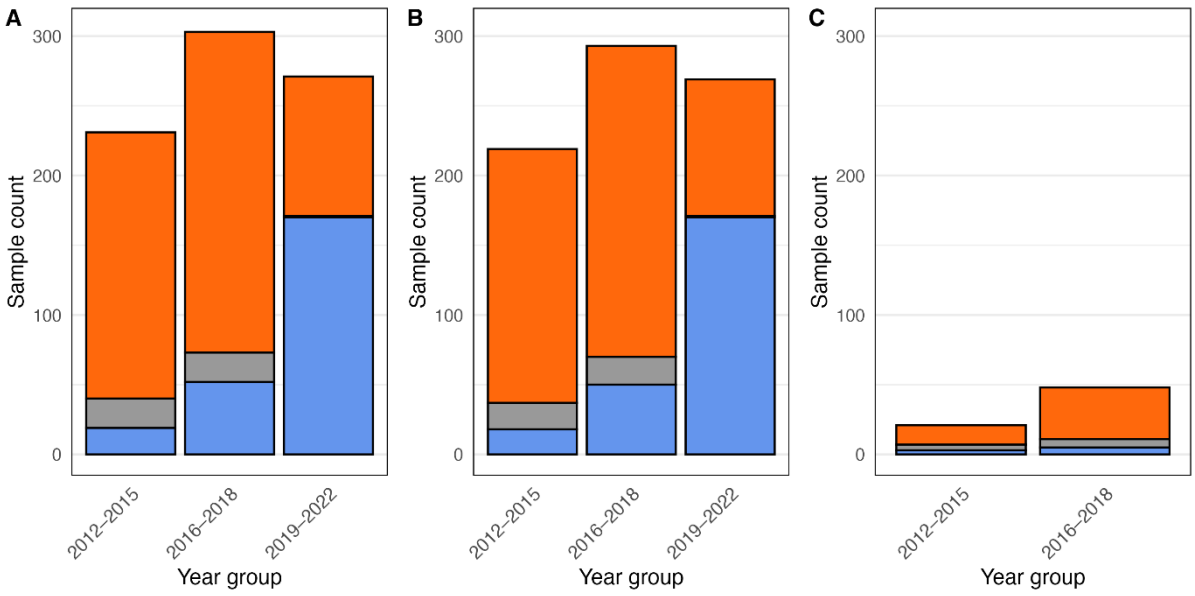

Extended Data Figure 21. Population ancestry composition among Brazilian Helicoverpa samples across three genomic datasets used for these analyses. (A) Genotype-likelihood dataset (n = 820 individuals), (B) variant-calling dataset (n = 796), and (C) haplotagging dataset (n = 93). Bars show absolute counts of individuals per year-group, coloured by ancestry group as determined by PCAngsd (armigera-like, zea-like, and early generation hybrid categories). All datasets include only Brazilian and newly sequenced individuals; additional published samples were excluded for consistency across panels. All individuals in the variant-calling dataset (B) are included in genotype-likelihood dataset (A).

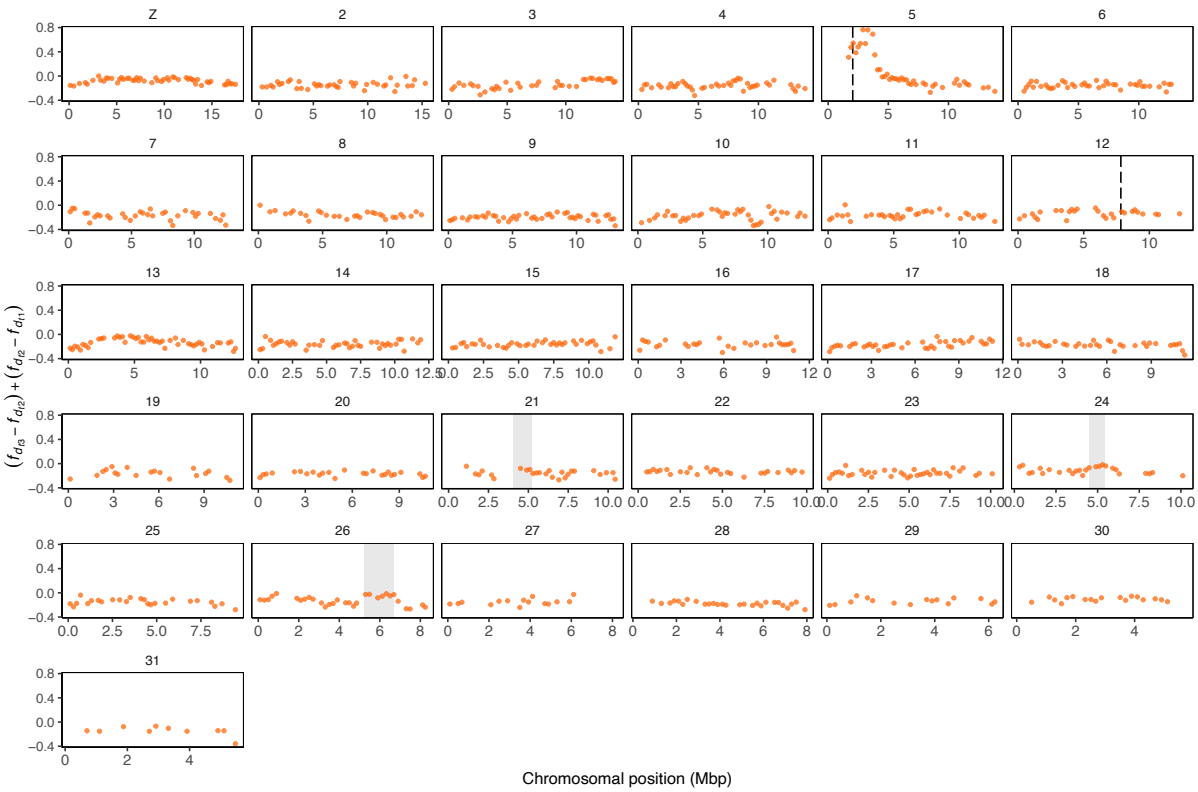

Extended Data Figure 22: Positive change in f_d over three timepoints, calculated in 200kbp windows with at least 500 usable sites per window for the topology (((ZEA, ZEA_BRAZIL), ARM)), PUN), *i.e.* gene flow from *H. armigera* to *H. zea*.

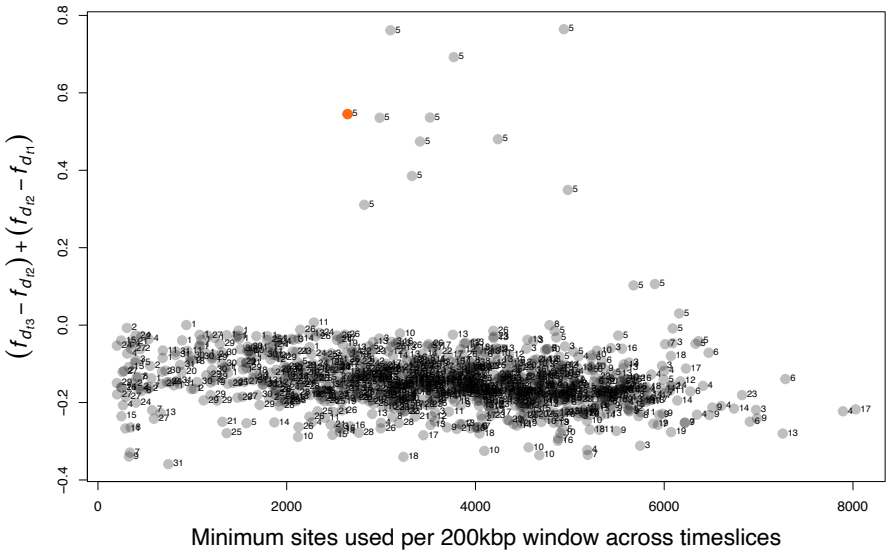

Extended Data Figure 23: Vertical axis: Positive change in f_d over three timepoints, calculated in 20kbp windows with at least 200 usable sites per window for the topology (((ZEA, ZEA_BRAZIL), ARM)), PUN), *i.e.* gene flow from *H. armigera* to *H. zea*. Horizontal axis: minimum number of sites used per window. Points are labelled with the chromosome on which the window occurs. The window on which *CYP337B3* occurs is highlighted in orange.

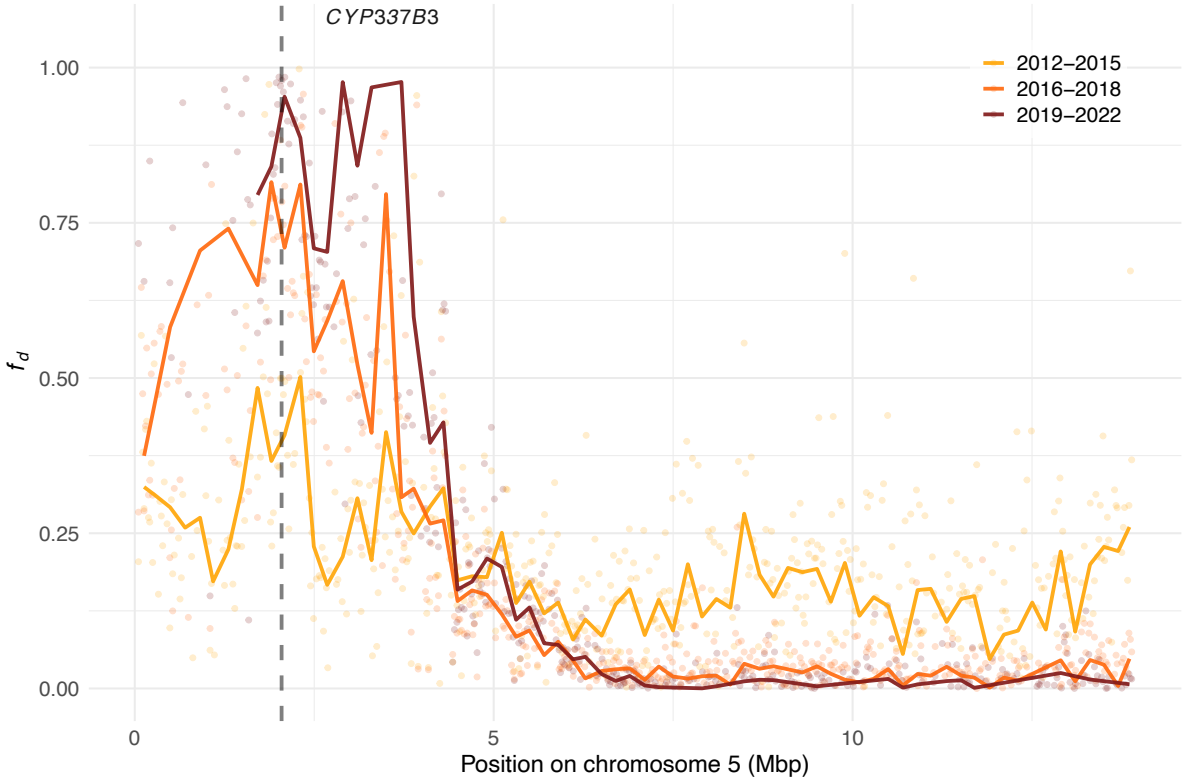

Extended Data Figure 24: f_d using the topology (((ZEA, ZEA_BRAZIL), ARM)), PUN), indicative of introgression from *H. armigera* to *H. zea*, shown for chromosome 5 for individuals split into three temporal sets. 200kbp windows with at least 500 usable sites shown as lines; 20kbp windows with at least 200 usable sites shown as points. Dasshed line indicates the position of *CYP337B3*.

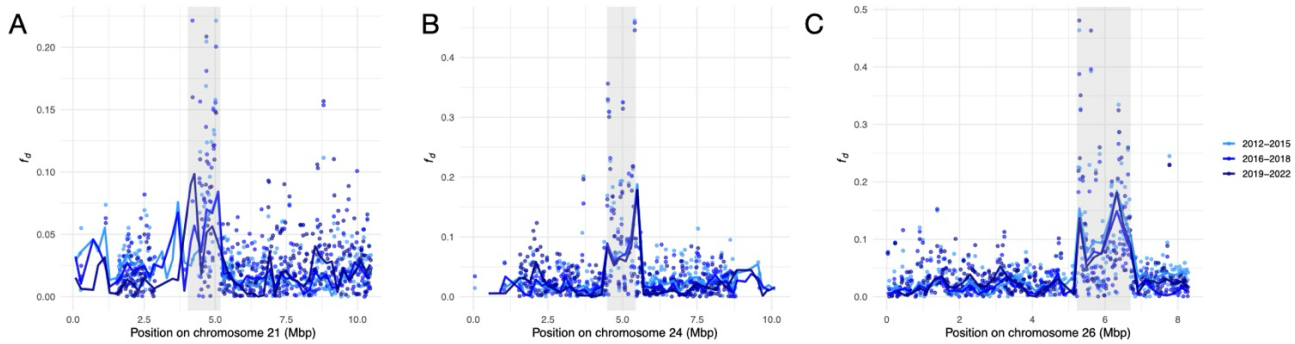

Extended Data Figure 25: f_d using the topology (((ARM, ARM_BRAZIL), ZEA)), PUN), indicative of introgression from *H. zea* to *H. armigera*, shown for chromosomes 21, 24, and 26 (A-C respectively), for individuals split into three temporal sets. f_d calculated in 200kbp windows (lines) and 20kbp windows (points), with inversion breakpoints inferred based on synteny comparisons displayed in grey. There is no apparent change in the introgression signal over time in the inversion regions.

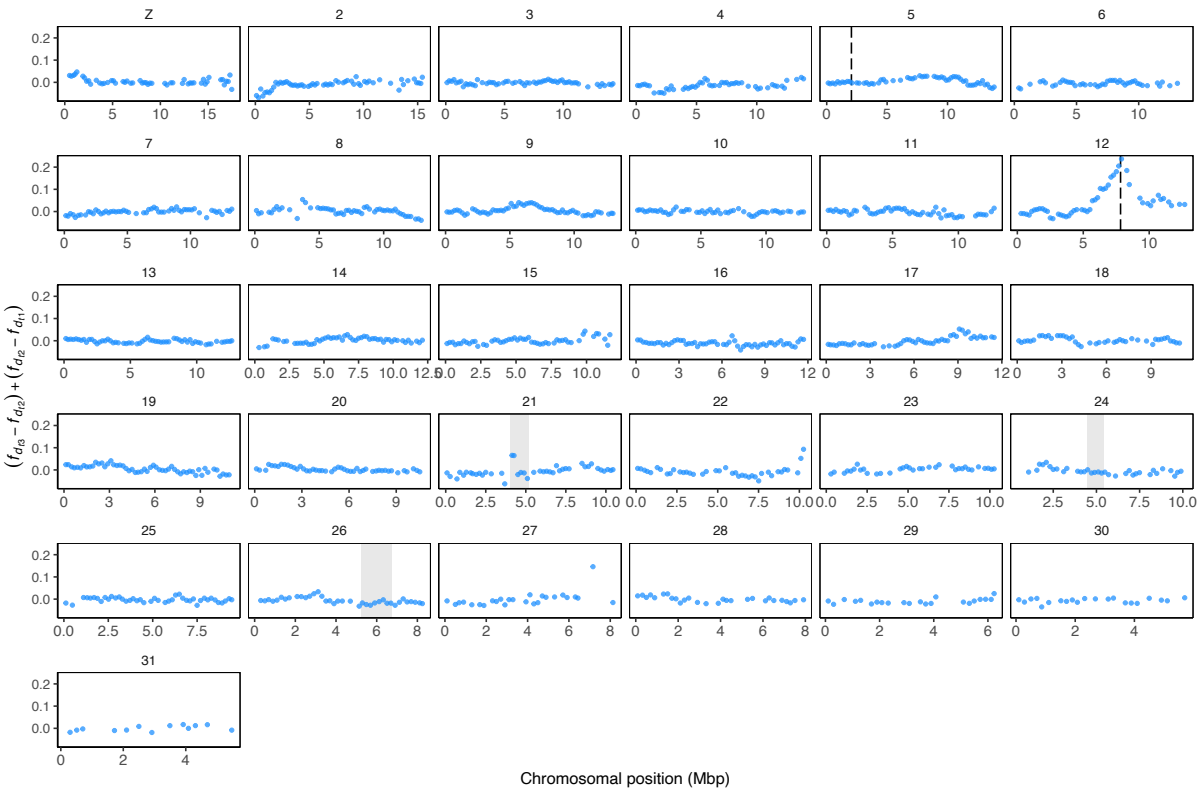

Extended Data Figure 26: Positive change in f_d over three timepoints, calculated in 200kbp windows with at least 500 usable sites per window for the topology (((ARM, ARM_BRAZIL), ZEA)), PUN), *i.e.* gene flow from *H. zea* to *H. armigera*.

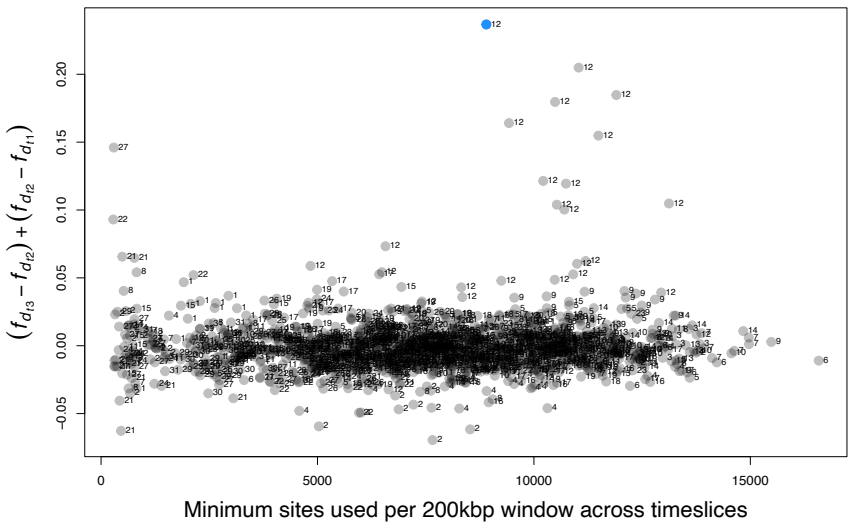

Extended Data Figure 27: Vertical axis: Positive change in f_d over three timepoints, calculated in 200kbp windows with at least 500 usable sites per window for the topology (((ARM, ARM_BRAZIL), ZEA)), PUN), *i.e.* gene flow from *H. zea* to *H. armigera*. Horizontal axis: minimum number of sites used per window. Points are labelled with the chromosome on which the window occurs. The window on which the trypsin allele cluster and the QTL for Bt resistance occurs is highlighted in blue.

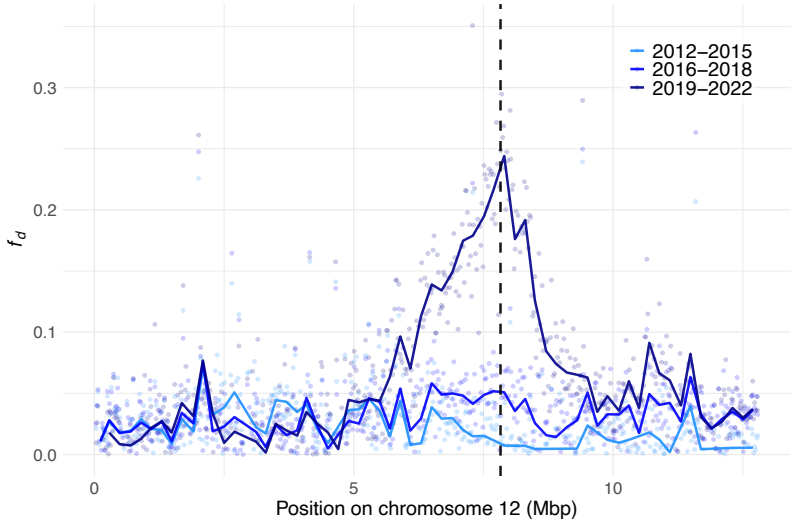

Extended Data Figure 28: f_d using the topology (((ARM, ARM_BRAZIL), ZEA)), PUN), indicative of introgression from *H. zea* to *H. armigera*, shown for chromosome 12 for individuals split into three temporal sets. 200kbp windows with at least 500 usable sites shown as lines; 20kbp windows with at least 200 usable sites shown as points. Dashed line indicates the position of the trypsin cluster.

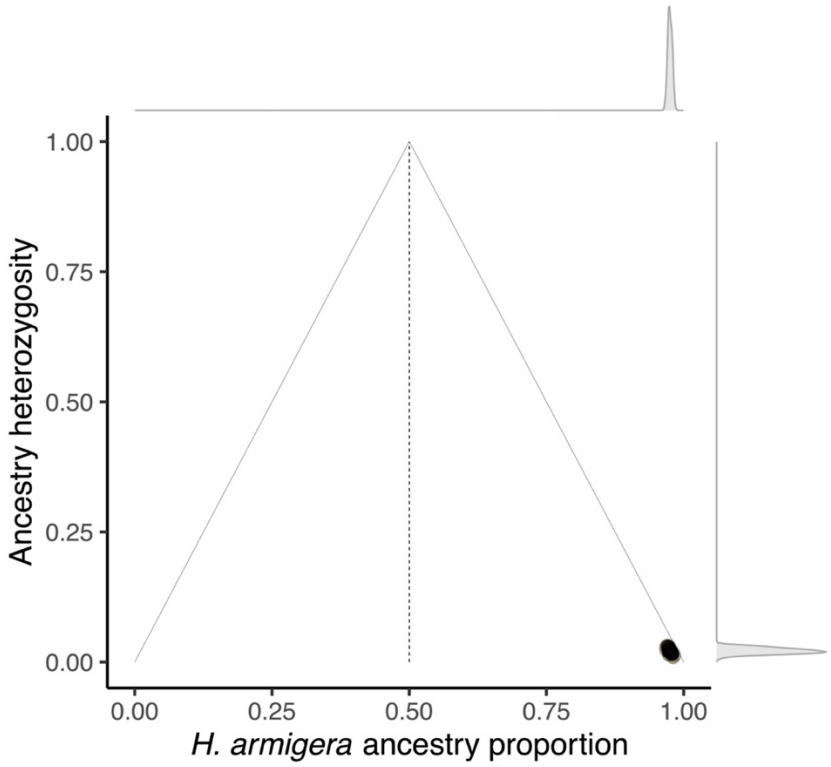

Extended Data Figure 29: Ancestry proportion and heterozygosity (as for Figure 1C) of QTL samples using Call Set 2; all individuals are *H. armigera* (minimum *H.* armigera ancestry proportion was 0.966, mean = 0.975).

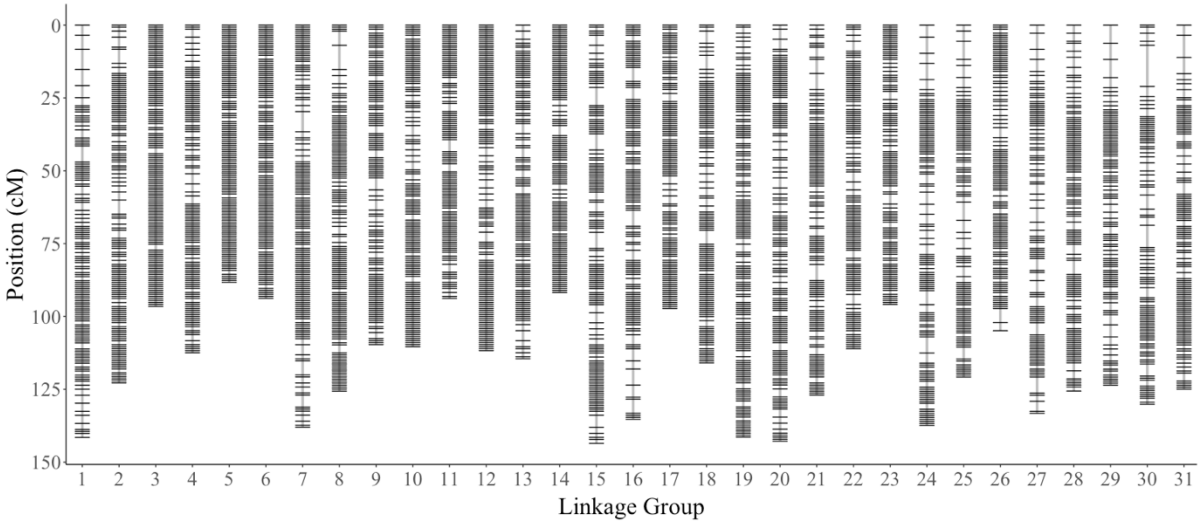

Extended Data Figure 30: Linkage map of F2 the intercross population, derived from the cross between the *Helicoverpa armigera* susceptible and the Cry1Ac resistant strains. Linkage groups are ordered along the horizontal axis. Each line in a linkage group denotes a marker, and the vertical axis shows the genetic position of markers in cM.

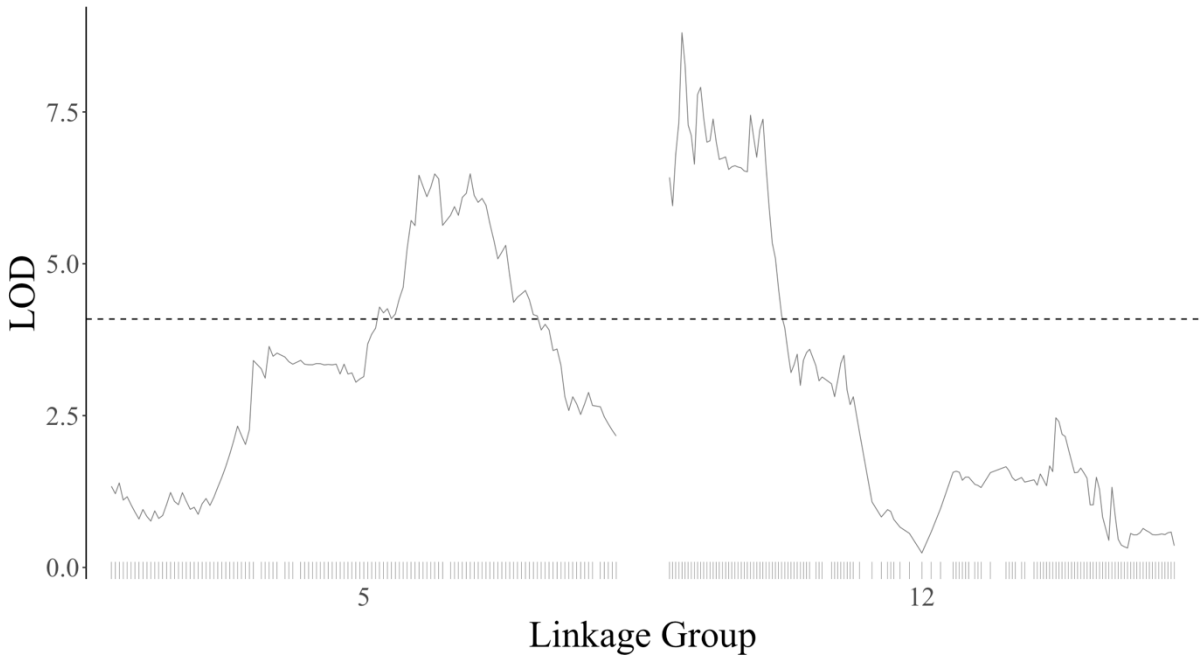

Extended Data Figure 31: The LOD profiles of linkage groups 5 and 12, where significant QTLs for the survival trait were identified. The Y-axis shows the LOD ratio, and the X-axis shows the linkage groups 5 and 12. The lines at the bottom of the linkage group denote markers.

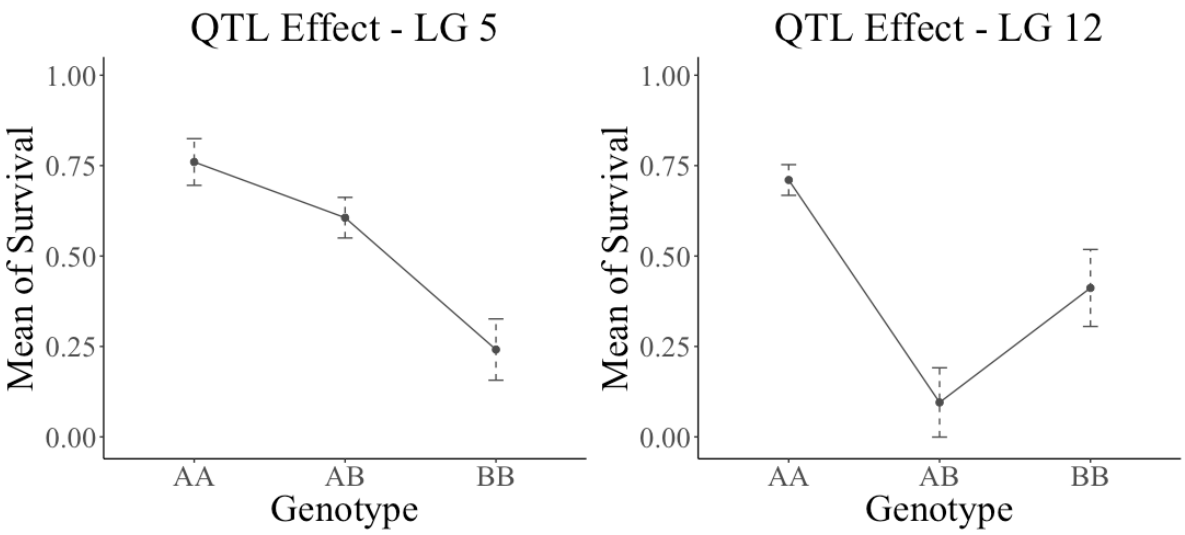

Extended Data Figure 32: Effect plot of the main QTL on linkage groups 5 and 12. The X-axis represents the genotypes homozygote resistant (AA), heterozygote (AB) and homozygote susceptible (BB). The Y-axis represents the phenotypic value (survival ratio) after a transformation using the logit function.

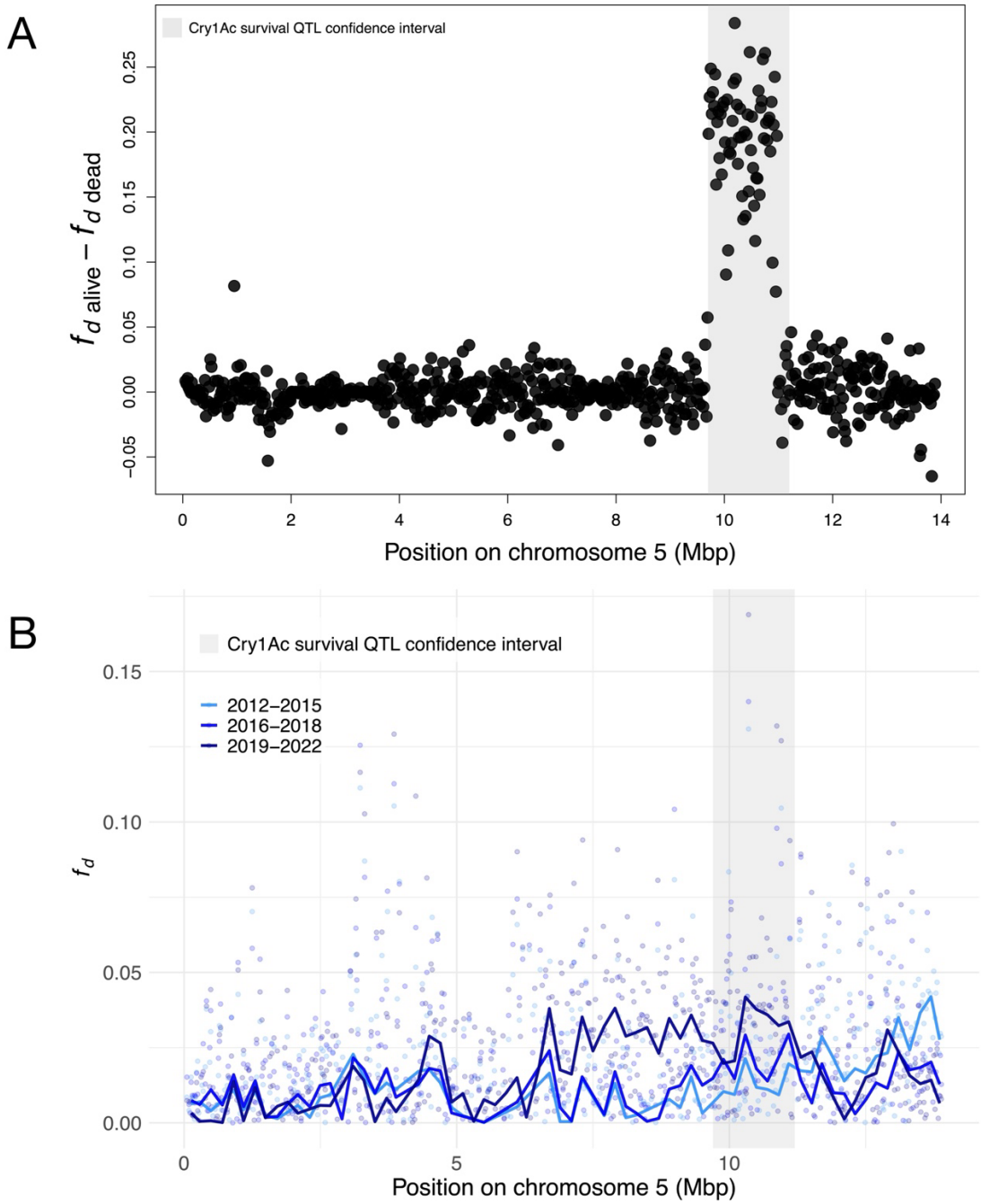

Extended Data Figure 33 A: Difference in the signal of *H. zea* allele sharing between alive and dead individuals. In both cases f_d was calculated using the topology (((ARM, QTL_SAMPLE), ZEA)), PUN). Grey shaded regions indicate the QTL confidence intervals. **B:** introgression from *H. zea* to *H. armigera* among wild samples divided into 3 timepoints, using the same test topology. Lines indicate 200kbp windows; points indicate 20kbp windows with at least 200 usable sites.